UNIVERSITÀ
DI PAVIA

Dipartimento di di Biologia e Biotecnologie "L. Spallanzani"

Master's Degree in Advanced Biotechnology

Department of Biotechnology and Food Science

CRISPR/Cas9-Mediated Mutagenesis of *Marchantia polymorpha MpTOLa* and *MpTOLb* and Complementation of the mutant lines with *Arabidopsis thaliana AtTOL1, AtTOL2, AtTOL6, and AtTOL9 genes.*

Mutagenesi mediata da CRISPR/Cas9 dei geni *MpTOLa* e *MpTOLb* di *Marchantia polymorpha* e Complementazione delle linee mutanti con i geni *AtTOL1, AtTOL2, AtTOL6,* e *AtTOL9* di *Arabidopsis thaliana.*

Supervisor:

Professor Alberta Pinnola

Co-supervisor:

Professor Barbara Korbei

Experimental Thesis by

Nicoletta Maria Zavtur

Academic Year 2025/2026

ABSTRACT

The endosomal trafficking system plays a fundamental role in the regulation of plasma membrane proteins and in their sorting towards recycling or degradation. In plants, ubiquitinated membrane proteins are recognised by the ESCRT machinery eventually delivered to the vacuole for degradation. The ESCRT complex is evolutionarily conserved in animals, fungi and plants and it is composed of several cytosolic protein complexes, called ESCRT-0, -I, -II and -III.

The ESCRT-0 complex, which is responsible for the recognition and interaction with ubiquitin, is absent in higher plants. Instead, TOL (Target of Myb1) proteins act as ubiquitin receptors during the early steps of the ESCRT pathway.

While *Arabidopsis thaliana* contains nine TOL proteins with partially redundant functions, the liverwort *Marchantia polymorpha* contains only two TOL homologues, MpTOLa and MpTOLb. This lower genetic redundancy, together with the predominantly haploid life cycle of *M. polymorpha*, makes this species a useful system for studying TOL protein function.

MpTOLa is more closely related to AtTOL1/AtTOL2, while MpTOLb shows similarities with AtTOL6/AtTOL9.

The aim of this study was therefore to investigate the role of MpTOLa and MpTOLb proteins in *M. polymorpha* by observing the phenotypes of mutant lines. CRISPR/Cas9 vectors containing two guide RNAs for each locus were used to introduce mutations into the targeted genes.

Stable mutations, that were maintained after vegetative propagation, were identified in two *Mptola* lines (*Mptola-1* and *Mptola-2*) and in three *Mptolb* lines (*Mptolb-5*, *Mptolb-6* and *Mptolb-8*).

Sequence analyses predicted two distinct types of mutations: the *Mptola* lines carried early frameshift mutations predicted to cause loss-of-function, whereas the *Mptolb* lines carried mutations predicted to result in C-terminal truncations, retaining the N-terminal core of the protein. However, their consequences for transcript and protein stability and function remain to be experimentally tested.

Phenotypic differences were observed between the mutant lines and their corresponding WT controls. Both *Mptola-1* and *Mptola-2* lines were smaller and showed asymmetric thallus development, including an approximately 90° rotation of one of the thallus lobes. *Mptola-1* also showed altered rhizoid growth and curled rhizoid tips, while *Mptola-2* showed a more vertical and hyponastic growth pattern.

The *Mptolb-5* plant showed wider thallus lobes and asymmetric development of the two lobes, with earlier development of the apical notch compared with the WT plant. *Mptolb-6* showed reduced growth, a strongly folded and compact thallus, with a pronounced three-dimensional structure. In *Mptolb-8* the apical notch was more pronounced than in the WT plant, and differences in thallus expansion became more evident during later development.

Differences in the timing of gemma cup formation were also observed.

The male mutant lines (*Mptola-1* and *Mptolb-6)* developed the gemma cups later than the corresponding male WT controls (Tak-1), while the female mutant lines (*Mptola-2, Mptolb-5* and *Mptolb-8)* developed them earlier than the female WT control (Tak-2).

These observations suggest that MpTOLa and MpTOLb may contribute to cell polarity, organogenesis, and developmental timing in *M. polymorpha*. Based on the known functions of TOL proteins in *Arabidopsis*, changes in the trafficking of proteins involved in auxin signalling could contribute to the altered growth phenotypes, while alterations in ABA-related trafficking could be involved in the differences observed in gemma cup formation. However, these possible relationships still require experimental verification.

A second part of the study focused on the generation of molecular tools for future complementation experiments of *MpTOLa* and *MpTOLb* with the *AtTOL1*, *AtTOL2*, *AtTOL6* and *AtTOL9* genes from *A. thaliana*. This will be important for studying whether *Arabidopsis* TOL proteins are able to complement the phenotypes of *M. polymorpha* TOL mutant lines and for analysing their subcellular localization. Expression vectors carrying AtTOL2 and AtTOL9 fused to a C-terminal GFP tag under the control of the constitutive promoter MpEF1ap (*MpEF1ap::AtTOL2-GFP* and *MpEF1ap::AtTOL9-GFP*) were successfully assembled. Completing the remaining constructs *MpEF1ap::AtTOL1-GFP*, *MpEF1ap::AtTOL6-GFP*, *MpEF1ap::MpTOLa-GFP* and *MpEF1ap::MpTOLb-GFP* would allow a more complete comparison of the different TOL proteins and their ability to complement the *M. polymorpha* mutant phenotypes.

Overall, the mutant lines and molecular tools generated in this study provide a basis for further investigating the roles of MpTOLa and MpTOLb in endosomal trafficking and their possible contribution to plant development in *M. polymorpha*, as well as for evaluating the evolutionary conservation of TOL-mediated sorting in land plants.

ABSTRACT - ITALIANO

Il sistema di traffico endosomiale svolge un ruolo fondamentale nella regolazione delle proteine della membrana plasmatica e nel loro smistamento verso il riciclo o la degradazione. Nelle piante, le proteine di membrana ubiquitinate vengono riconosciute dal complesso ESCRT e potenzialmente indirizzate al vacuolo per la successiva degradazione.

Il complesso ESCRT è evolutivamente conservato negli animali, nei funghi e nelle piante ed è composto da diversi complessi proteici citosolici, chiamati ESCRT-0, -I, -II e -III.

Il complesso ESCRT-0, responsabile del riconoscimento e dell'interazione con l'ubiquitina, è assente nelle piante superiori. Al suo posto, le proteine TOL (Target of Myb1) agiscono come recettori dell'ubiquitina durante le prime fasi della via ESCRT.

Mentre *Arabidopsis thaliana* contiene nove proteine TOL con funzioni parzialmente ridondanti, il muschio epatico *Marchantia polymorpha* contiene solo due omologhi TOL, MpTOLa e MpTOLb. Questa minore ridondanza genetica, insieme al ciclo vitale prevalentemente aploide di *M. polymorpha*, rende questa specie un sistema utile per lo studio della funzione delle proteine TOL.

MpTOLa è più strettamente correlata ad AtTOL1/AtTOL2, mentre MpTOLb mostra somiglianze con AtTOL6/AtTOL9.

Lo scopo di questo studio era quindi quello di investigare il ruolo delle proteine MpTOLa e MpTOLb in *M. polymorpha* attraverso l'osservazione dei fenotipi delle linee mutanti. Sono infatti stati utilizzati vettori CRISPR/Cas9 contenenti due RNA guida per ciascun locus, al fine di introdurre mutazioni nei geni bersaglio.

Sono state identificate mutazioni stabili, mantenute dopo la propagazione vegetativa, in due linee *Mptola* (*Mptola-1* e *Mptola-2*) e in tre linee *Mptolb* (*Mptolb-5*, *Mptolb-6* e *Mptolb-8*).

Le analisi delle sequenze hanno mostrato due tipi distinti di mutazioni: le linee *Mptola* presentavano mutazioni frameshift precoci, previste come causa di una perdita di funzione, mentre le linee *Mptolb* presentavano mutazioni previste come responsabili di troncamenti C-terminali, mantenendo lo scheletro N-terminale della proteina. Tuttavia, le loro conseguenze sulla stabilità del trascritto e della proteina e sulla loro funzione devono ancora essere verificate sperimentalmente.

Sono state osservate differenze fenotipiche importanti tra le linee mutanti e i rispettivi controlli wild-type (WT). Entrambe le linee *Mptola-1* e *Mptola-2* erano più piccole e mostravano uno sviluppo asimmetrico del tallo, inclusa una rotazione di circa 90° di uno dei lobi del tallo. *Mptola-1*

mostrava inoltre una crescita alterata dei rizoidi e apici dei rizoidi arricciati, mentre *Mptola-2* mostrava una crescita più verticale e un orientamento iponastico.

La pianta *Mptolb-5* mostrava lobi del tallo più ampi e uno sviluppo asimmetrico dei due lobi, con uno sviluppo più precoce dell'incisione apicale rispetto alla pianta WT. *Mptolb-6* mostrava una crescita ridotta e un tallo fortemente ripiegato e compatto, con una pronunciata struttura tridimensionale. In *Mptolb-8*, l'incisione apicale era più accentuata rispetto alla pianta WT e le differenze nell'espansione del tallo diventavano più evidenti durante le fasi successive dello sviluppo. Sono state inoltre osservate differenze nella tempistica di formazione delle coppe gemmifere. Le linee mutanti maschili (*Mptola-1* e *Mptolb-6*) sviluppavano le coppe gemmifere più tardi rispetto ai corrispondenti controlli WT maschili (Tak-1), mentre le linee mutanti femminili (*Mptola-2*, *Mptolb-5* e *Mptolb-8*) le sviluppavano prima rispetto al controllo WT femminile (Tak-2). Queste osservazioni suggeriscono che MpTOLa e MpTOLb possano contribuire alla polarità cellulare, all'organogenesi e alla tempistica dello sviluppo in *M. polymorpha*. Sulla base delle funzioni note delle proteine TOL in *Arabidopsis*, cambiamenti nel traffico di proteine coinvolte nella segnalazione dell'auxina potrebbero contribuire ai fenotipi di crescita osservati, mentre alterazioni nel traffico correlato all'ABA potrebbero essere coinvolte nelle differenze osservate nella formazione delle coppe gemmifere. Tuttavia, queste possibili relazioni richiedono ancora una verifica sperimentale.

Una seconda parte dello studio si è concentrata sulla generazione di strumenti molecolari per futuri esperimenti di complementazione di *MpTOLa* e *MpTOLb* con i geni *AtTOL1*, *AtTOL2*, *AtTOL6* e *AtTOL9* di *A. thaliana*. Questi esperimenti saranno importanti per studiare se le proteine TOL di *Arabidopsis* siano in grado di complementare i fenotipi delle linee mutanti TOL di *M. polymorpha* e per analizzarne la localizzazione subcellulare. Sono stati assemblati con successo vettori di espressione contenenti AtTOL2 e AtTOL9 fusi a un tag GFP C-terminale, sotto il controllo del promotore costitutivo MpEF1ap (*MpEF1ap::AtTOL2-GFP* e *MpEF1ap::AtTOL9-GFP*). Il completamento dei costrutti rimanenti *MpEF1ap::AtTOL1-GFP*, *MpEF1ap::AtTOL6-GFP*, *MpEF1ap::MpTOLa-GFP* e *MpEF1ap::MpTOLb-GFP* permetterebbe un confronto più completo delle diverse proteine TOL e della loro capacità di complementare i fenotipi mutanti di *M. polymorpha*.

Nel complesso, le linee mutanti e gli strumenti molecolari generati in questo studio forniscono una base per ulteriori studi sui ruoli di MpTOLa e MpTOLb nel traffico endosomiale e sul loro possibile contributo allo sviluppo di *M. polymorpha*, nonché per valutare la conservazione evolutiva dei meccanismi di smistamento mediati dalle proteine TOL nelle piante terrestri.

SUMMARY

1. INTRODUCTION **9**

1.1 The endosomal system of plants ***9***

1.2 Ubiquitination of plasma membrane proteins in plants ***11***

1.3 The ESCRT machinery ***12***

1.4 TOL proteins in higher plants ***13***

1.5 Marchantia polymorpha ***15***

1.6 TOL proteins in Marchantia polymorpha ***18***

2. AIM OF THE STUDY **21**

3. MATERIALS AND METHODS **22**

3.1 Materials ***22***

3.1.1 Growth Media *22*

3.1.2 Solutions and Buffers *23*

3.1.3 Plasmids used *26*

3.1.4 Bacterial strains used *26*

3.2 Plant Methods ***27***

3.2.1 Growth Conditions of Marchantia polymorpha *27*

3.2.2 Agrobacterium-mediated Transformation of Marchantia polymorpha *27*

3.2.3 Transfer of Marchantia polymorpha to Soil *28*

3.2.4 Gemmae Sterilisation *29*

3.2.5 Marchantia polymorpha Gemmae Propagation *29*

3.2.6 Plant Genomic DNA Extraction Using the CTAB Method *30*

3.3 Bacterial Methods ***31***

3.3.1 Preparation of Agrobacterium tumefaciens (or Escherichia coli) Electrocompetent Cells *31*

3.3.2 Electroporation into Competent A. tumefaciens (or E. coli) cells *32*

3.3.3 Heat Shock Transformation of E. coli *32*

3.3.4 Plasmid DNA Extraction *33*

3.3.5 Blue/White Screening of Positive Clones *33*

3.3.6 Glycerol Stock Preparation *33*

3.4 Molecular Biology Methods ***34***

3.4.1 PCR *34*

3.4.2 List of Primers Used *36*

3.4.3 Agarose Gel Electrophoresis *37*

3.4.4 DNA Purification *37*

3.4.5 DNA Gel Extraction *37*

3.4.6 DNA Quantification *38*

3.4.7 Restriction Enzyme Digestion *38*

3.4.8 Ligation *39*

3.4.9 Gateway Cloning: LR Reaction *40*

3.4.10 DNA Sample Preparation for Sanger Sequencing *40*

4. RESULTS AND DISCUSSION **42**

4.1 CRISPR/Cas9-mediated generation of MpTOLa and MpTOLb mutant candidates ***42***

4.2 Selection and molecular characterization of putative M. polymorpha MpTOLa and MpTOLb mutant lines ***43***

4.2.1 Molecular screening of the MpTOLa locus *44*

4.2.2 Molecular screening of the MpTOLb locus *46*

4.3 Characterization of M. polymorpha MpTOLa and MpTOLb mutant lines ***47***

4.4 Phenotypic characterization of M. polymorpha MpTOLa and MpTOLb mutant lines 52

4.5 Biological Rationale and Putative Molecular Mechanisms 67

4.5.1 Possible involvement of auxin transport in the growth phenotypes 67

4.5.2 Possible role of ABA signalling in developmental timing 68

4.6 Construction of MpTOL Expression Vectors for Cross-Species Functional Analysis 69

4.6.1 Initial Attempts to Replace the 35S Promoter 70

4.6.2 Revised Cloning Strategy and Construction of MpTOL Expression Vectors 71

5. CONCLUSIONS 72

6. REFERENCES 75

1. INTRODUCTION

1.1 The endosomal system of plants

The presence and localization of proteins within the plasma membrane (PM) inevitably influence plant development and contribute to the adaptation to continuously changing environmental conditions, including those associated with climate change. This is because the PM represents the interface between the inside and the outside of the cell and it is densely populated with proteins responsible for sensing and transmitting external stimuli. Therefore, plants must be able to rapidly and accurately regulate the abundance of their PM proteins (Paez Valencia et al., 2016).

The composition of PM proteins also depends on the developmental stage of the plant, and the continuous remodeling of membrane proteins promotes adaptation to environmental changes. In this context, the endocytic pathway plays a key role. It consists of a network of intracellular routes involved in the sorting, recycling, and degradation of PM proteins in plants (Schwihla and Korbei, 2020; Figure 1).

Together with the secretory pathway, which is responsible for the biosynthetic transport of proteins from the endoplasmic reticulum to the PM via the trans-Golgi network (TGN), the endocytic pathway, which is responsible for internalizing proteins from the PM, represents one of the major trafficking pathways of the plant endomembrane system (Aniento et al., 2022).

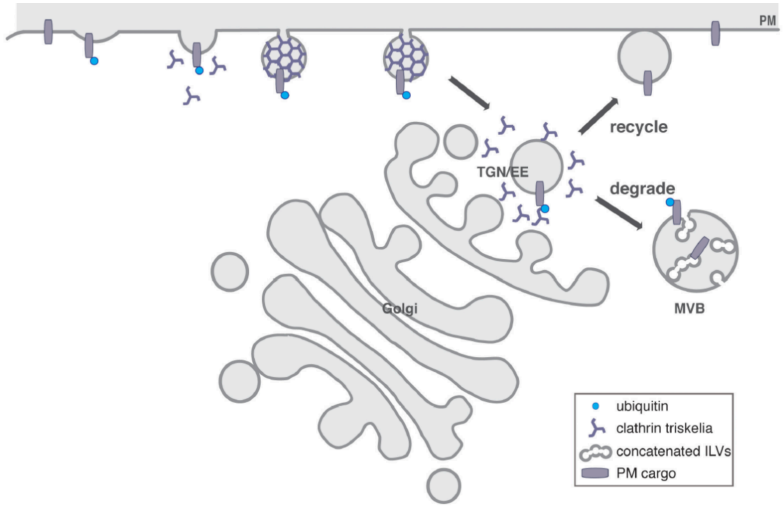


Figure 1: Clathrin-mediated endocytosis is a vesicular trafficking process through which transmembrane proteins are internalized into clathrin-coated vesicles (CCVs) and transported to the TGN for subsequent processing (Schwihla and Korbei, 2020).

The removal of PM-associated proteins requires a series of complex processes starting with clathrin-mediated endocytosis, which is the most common type of endocytosis in plants (Narasimhan et al., 2020). It is named after the coat protein clathrin, which self-assembles into structures known as triskelia. These structures interact with adaptor proteins and form a coat around the membrane invagination, giving rise to the so-called clathrin-coated pit (CCP). Clathrin-mediated endocytosis depends on adaptor proteins for cargo recruitment, since clathrin itself lacks the ability to bind cargo or membrane directly. Adaptor proteins directly interact with the cargo, which is recognized through specific sorting signals. Among these, ubiquitination is one of the most interesting and studied signals in plants. The detachment of the CCP from the PM is mediated by dynamins and dynamin-related proteins, which belong to the GTPase family, leading to the formation of a clathrin-coated vesicle (CCV). The CCV subsequently undergoes progressive uncoating during its transport towards the TGN (Figure 1) (Mattson et al., 2026).

In plants, the TGN functions both as a central sorting compartment and as an early endosome, directing endocytosed proteins either back to the PM for recycling, thus enabling rapid responses to environmental changes, or towards the vacuole for degradation (Paez Valencia et al., 2016; Reynolds et al., 2018). Membrane proteins destined for degradation, rather than recycling, are subsequently sorted into intraluminal vesicles (ILVs) at the limiting membrane of the multivesicular bodies (MVBs), a process that requires their ubiquitination and recognition by the Endosomal Sorting Complex Required for Transport (ESCRT) machinery (Buono et al., 2017) (Figure 1). MVBs subsequently fuse with the tonoplast, the single membrane surrounding the vacuole, releasing their ILVs into the vacuolar lumen. Within the vacuole, proteases and lipases degrade proteins and membranes into their basic components (Frankel and Audhya, 2018).
Although the precise mechanisms underlying endocytosis of membrane proteins in plants are not yet fully understood, it is well established that ubiquitin acts as a key signal in this process.

1.2 Ubiquitination of plasma membrane proteins in plants

Plants, as sessile organisms, have developed multiple mechanisms to rapidly respond to their surrounding environment. A process that plays a crucial role in the degradation of membrane proteins is their covalent modification by ubiquitin. This modification, known as ubiquitination, is a reversible post-translational process that is essential for the proper sorting of PM proteins into degradative compartments such as the vacuole (Schwihla and Korbei, 2020). Ubiquitination is associated with the three main protein degradation pathways: the proteasome, the vacuole/ lysosome, and the autophagosome. It contributes to the regulation of protein half-life (Clague and Urbé, 2010; Korbei and Luschnig, 2013; Zientara-Rytter and Sirko, 2016), but also influences the localization, activity, and interactions of many proteins (Komander and Rape, 2012). Proteins can undergo monoubiquitination, multi-monoubiquitination, or polyubiquitination. Accordingly, ubiquitin can form either linear or branched chains through linkage to its N-terminal end or to internal lysine residues (K6, K11, K27, K29, K33, K48, and K63) of other ubiquitin molecules (Husnjak and Dikic, 2012).

Consequently, multiple types of ubiquitination exist, all of which are highly complex in plants, involving more than 1500 ubiquitin–protein ligases (Hua and Vierstra, 2011). Each type of ubiquitination differently influences the fate of the target proteins (Komander and Rape, 2012).

The decoding of ubiquitin signals is mediated by ubiquitin receptors, which are proteins containing ubiquitin-binding domains (UBDs) that bind ubiquitin non-covalently. These domains consist of short amino acid sequences lacking a strict consensus motif and typically display low binding affinity for ubiquitin (Husnjak and Dikic, 2012). To date, the full functional diversity and significance of ubiquitination are not yet completely understood. To gain deeper insight into this process, it is essential to investigate the role of ubiquitin receptors, which are able to translate the ubiquitin signal into specific cellular responses.

Nevertheless, the presence of ubiquitin on PM proteins is considered sufficient to direct their sorting (Herberth et al., 2012; Martins et al., 2015). Both monoubiquitination and K63-linked polyubiquitination are involved in the endocytic trafficking of PM proteins into the vacuolar lumen, where they are subsequently degraded (Figure 2; Lauwers et al., 2009; Erpapazoglou et al., 2014; Piper et al., 2014).

1.3 The ESCRT machinery

Ubiquitinated PM proteins are internalized as endocytic cargo, and delivered to the TGN, which in plants also functions as an early endosome (Dettmer et al., 2006). Once internalized, proteins can follow two main routes: they can either be deubiquitinated and recycled back to the PM or targeted to the vacuole through the action of multiprotein complexes known as ESCRT (endosomal sorting complexes required for transport) machinery (Figure 2; Schwihla and Korbei, 2020).

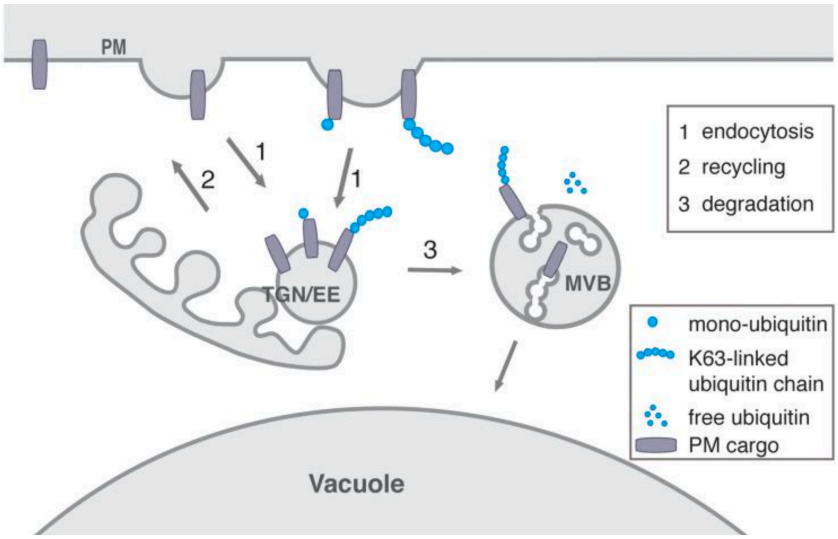


Figure 2: Schematic representation of how ubiquitinated proteins are recruited during membrane invagination (1) and subsequently directed either towards recycling (2) or internalization into multivesicular bodies (MVBs) for degradation (3) (Schwihla and Korbei, 2020).

The ESCRT machinery consists of several cytosolic protein complexes, termed ESCRT-0, -I, -II, and -III together with accessory proteins, and represents a key system for recognition of membrane-associated cargo destined for degradation, as well as membrane remodeling required for the biogenesis of MVBs (Henne et al., 2011).

This highly conserved machinery functions also in plants, where it recognizes and sequesters ubiquitinated proteins, directing them into ILVs of MVBs (Gao et al., 2017; Isono and Kalinowska, 2017).

ESCRT complexes, in particular ESCRT-0, I and II contain subunits with UBDs, which anchor ubiquitinated cargo and guide it through the endocytic degradation pathway (Korbei, 2022). In

animals and fungi, the ESCRT-0 complex is made up of two subunits and contains multiple UBDs which show a preference for K63-linked polyubiquitin chains, while its FYVE domain mediates binding to phosphatidylinositol 3-phosphate, anchoring the complex to the endosomal membrane and thus initiates the endocytic sorting pathway. After concentrating ubiquitinated cargo, ESCRT-0 recruits ESCRT-I, which subsequently interacts with ESCRT-II (Hurley, 2010).

The cargo-enriched domain generated by ESCRT-I and ESCRT-II promotes membrane invagination towards the endosomal lumen. In contrast to the other ESCRT complexes, ESCRT-III does not possess UBDs and is involved in cargo deubiquitination via deubiquitinating enzymes (DUBs), as well as in membrane scission during sorting and incorporation into ILVs. Furthermore, ESCRT-III assemblies are thought to prevent the escape of trapped cargo by forming connections between ILVs budding into the lumen of MVBs (Isono and Kalinowska, 2017; Schwihla and Korbei, 2020).

1.4 TOL proteins in higher plants

In plants, the ESCRT system is composed of ESCRT-I, ESCRT-II, and ESCRT-III, while ESCRT-0 is absent (Liu et al., 2022). Evolutionarily conserved ubiquitin receptors, known as TOL (Target of Myb1 (TOM1)) proteins, function as substitutes for the ESCRT-0 machinery, as they are responsible for recognizing and capturing ubiquitinated cargo (Korbei et al., 2013). Structurally, TOL proteins resemble the ESCRT-0 subunits of mammalian and yeast systems, containing two N-terminal UBDs, the VHS (Vps27/Hrs/STAM) and GAT (GGA and TOM1) domains, followed by an unstructured, intrinsically disordered (IDR) C-terminal domain (Figure 3). This conservation of domain architecture suggests that the mechanism of ubiquitinated cargo capture at the ESCRT-0 level has been maintained across kingdoms, despite the divergence of the receptor proteins themselves (Wang et al., 2010). The VHS and GAT domains are involved in the recognition and binding of ubiquitinated cargo (Moulinier-Anzola et al., 2020). Both domains are highly structured, with the VHS domain forming an eight-helix superhelix and the GAT domain adopting a three-helix bundle structure. They interact with ubiquitin chains and other adaptor proteins, thereby contributing to the recognition and sorting of ubiquitinated membrane proteins for transport to endosomes (Misra et al., 2000; Akutsu et al., 2005).

The VHS domain has been proposed to act as a “recognition and anchoring module”, contributing to cargo recognition and promoting association with membranes and vesicles (Lohi et al., 2002).

During plant evolution, this protein family has expanded, giving rise to nine members in the model plant *Arabidopsis thaliana*, referred to as TOM1-like (TOL) proteins with a similar structure, N-terminal ubiquitin-binding VHS and GAT domains followed by C-terminal IDRs of different lengths (Figure 3).

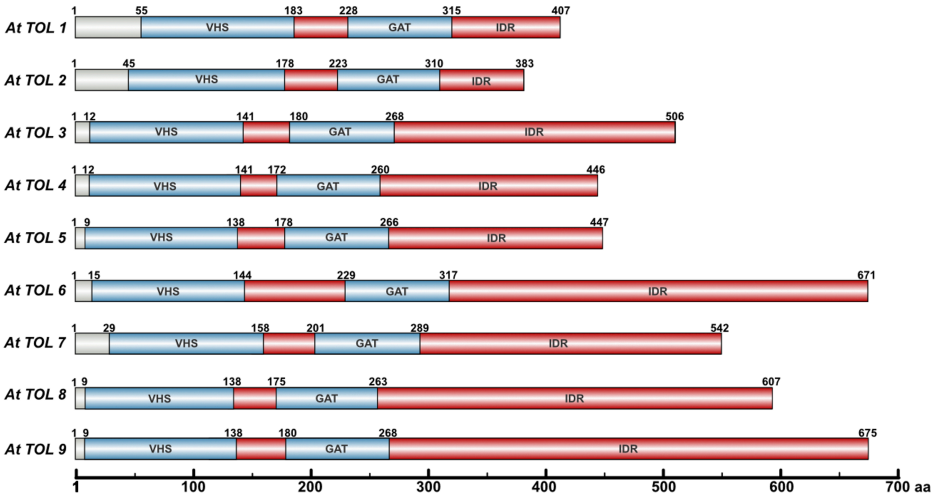


Figure 3: *In silico* analysis of the domain organization of the nine TOL proteins in *Arabidopsis thaliana.* The N-terminal UBDs, the VHS and GAT domains are indicated in blue, while the C-terminal IDR is in red.

It has also been shown that TOL proteins can act as multivalent ubiquitin receptors during the early stages of ESCRT-mediated protein degradation, facilitating the transport of ubiquitinated cargo to the vacuole (Moulinier-Anzola et al., 2020). While the TOL family has been extensively characterized in *Arabidopsis*, its functional conservation across land plants remains largely unexplored. Individual TOL members appear to have diversified functionally, for instance, in ABA signaling (Moulinier-Anzola et al., 2024), despite considerable redundancy within the family, as higher-order mutants are typically required to uncover clear phenotypes (Korbei et al., 2013) but show differences in their localization (Moulinier-Anzola et al., 2020). *Marchantia polymorpha*, as a bryophyte occupying a key phylogenetic position for studying the evolution of endocytic regulation, offers a unique system to determine whether this redundancy-diversification pattern is an ancestral feature of TOL-mediated sorting or a later innovation within vascular plants.

1.5 *Marchantia polymorpha*

Marchantia polymorpha is a widespread liverwort with a cosmopolitan distribution, predominantly found in temperate regions. The species has a long history of use in plant research and was already known in ancient Greece, where it was used in traditional medicine for the treatment of various diseases. By the 19th century, *M. polymorpha* had become one of the most extensively studied species in plant science. Its developing thalli, sporelings (young plants germinated from spores), and gemmalings (young plants derived from gemma) have been used for nearly two centuries to investigate morphological and physiological responses to different environmental conditions (Figure 4; Shimamura, 2016).

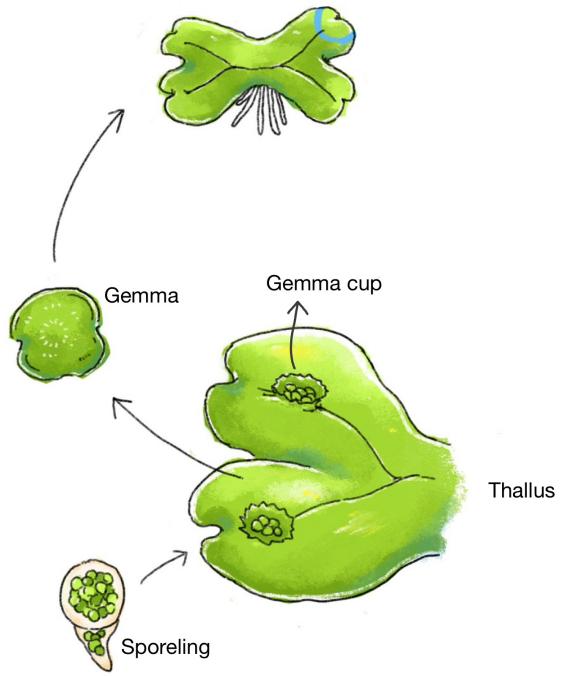


Figure 4: The body plan of *Marchantia polymorpha* (Kato et al., 2020)

Among liverworts, *M. polymorpha* is currently one of the most widely used model organisms. Its suitability for experimental studies is largely due to its simple thalloid morphology, short life cycle, and ease of cultivation and genetic manipulation. In addition, its predominantly haploid, gametophyte-dominant life cycle is particularly advantageous for genetic studies, in particular reverse genetics, as loss-of-function phenotypes are immediately apparent and not masked by allelic redundancy, allowing a more direct relationship between genotype and phenotype (Bowman et al.,

2017; Kohchi et al., 2021). This is a feature that has been widely exploited in CRISPR/Cas9-based functional studies.

Throughout most of its life cycle, *M. polymorpha* exists as a haploid gametophyte and this stage constitutes the dominant, photosynthetically active phase of the plant, forming a flattened, dichotomously branching thallus. During vegetative growth, it can reproduce asexually through the formation of gemmae, small, lens-shaped clonal propagules that are genetically identical to the parent plant, which develop in specialized structures known as gemma cups, which are arranged along the dorsal midline of the thallus (Figure 4) (Kato et al., 2020). This asexual pathway allows for rapid and efficient clonal propagation under favorable growth conditions and is the primary means by which *M. polymorpha* is maintained and propagated in laboratory culture (Berger et al., 2016).

Sexual reproduction can be induced by changes in light quality, leading to the development of distinct male and female reproductive structures (Figure 5; Berger et al., 2016; Kato et al., 2020). Fertilization is dependent on the presence of water, as the flagellated sperm must swim from the antheridia to reach the archegonia housing the eggs. Male gametangia (antheridia) develop on antheridiophores, while female gametangia (archegonia) form on archegoniophores. Both are stalked, umbrella-shaped structures that elevate the reproductive organs above the vegetative thallus. Following fertilization, the diploid zygote develops into a short-lived sporophyte that remains attached to and nutritionally dependent on the maternal gametophyte. Within the sporophyte, meiosis gives rise to haploid spores, which are released and germinate to re-establish the vegetative gametophyte, thereby completing the life cycle (Figure 5; Berger et al., 2016; Bowman, 2022).

Today, *Marchantia polymorpha* is widely used as a model system to investigate fundamental biological processes and to better understand evolutionary biology. Its genome, approximately 225 Mb in size, has been fully sequenced. It is relatively compact and shows low genetic redundancy compared to vascular plants, while still retaining a core set of genes involved in development, metabolism, and stress responses. This makes it a powerful and tractable system for functional annotation (Bowman et al., 2017).

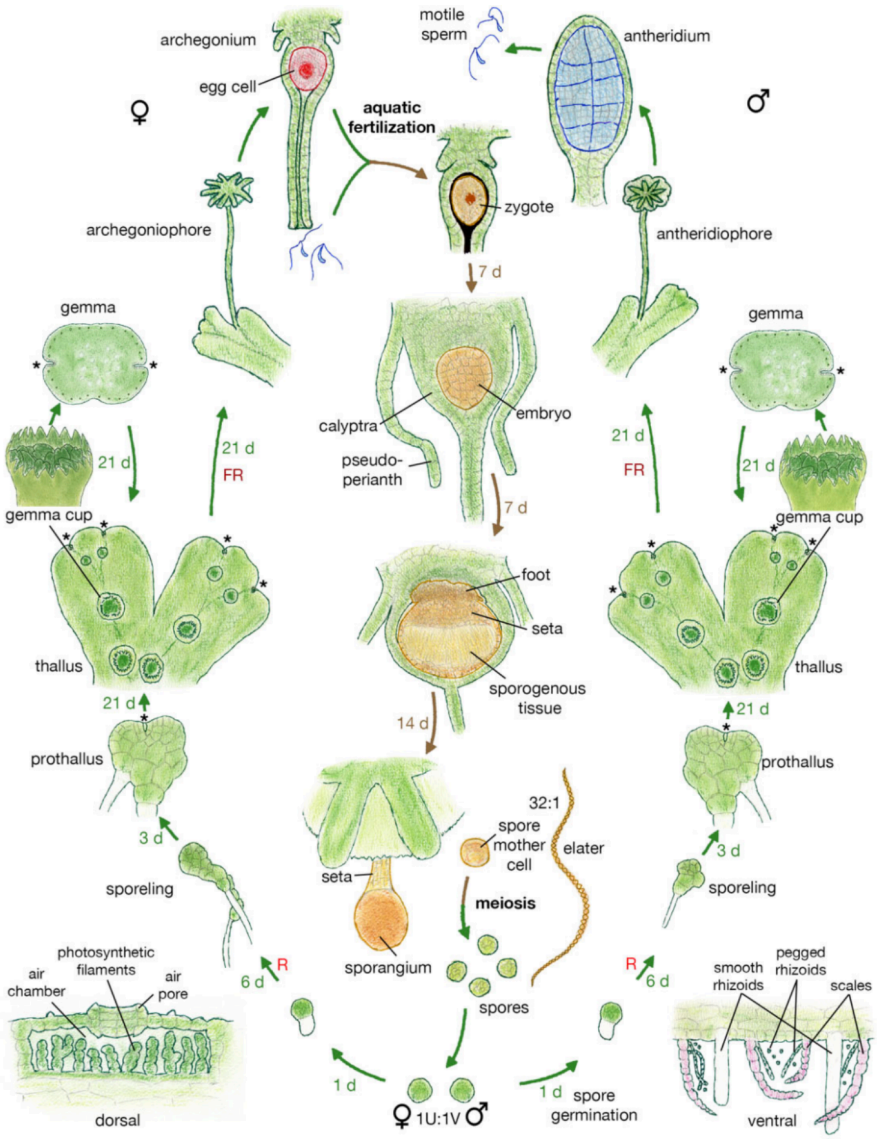


Figure 5: Life cycle of *M. polymorpha*. The haploid stages of the life cycle are depicted in shades of green, except for the female and male gametes; diploid stages of the life cycle are depicted in shades of brown. Gametophytic vegetative growth is largely indistinguishable between males and females, but this is not the case for all liverworts. Asterisks mark the apical meristems during the vegetative stages of the life cycle. Lower left and lower right show cross-sections of the dorsal (left) and ventral (right) regions of the complex thallus. Approximate times for the transitions between stages under optimal growth conditions are listed in days (d). R, red light; FR, far-red light (Bowman, 2022)

1.6 TOL proteins in *Marchantia polymorpha*

Marchantia polymorpha possesses a conserved ESCRT machinery including ESCRT-I, ESCRT-II, and ESCRT-III, as is characteristic of eukaryotes in general (Leung, Dacks & Field, 2008), though with lower genetic redundancy compared to *Arabidopsis thaliana* (Liu et al., 2022, Figure 6). This is particularly visible for the ESCRT-0 machinery where *Marchantia* contains only two TOL proteins, which we named TOLa and TOLb, compared to the nine TOLs in *Arabidopsis* (Figure 6). In *Arabidopsis thaliana*, these nine TOL proteins can be divided further into two groups according to their N-terminal stretch before their VHS and GAT domains and short C-terminal IDRs, where TOL1 and TOL2 belong to the first group, whereas TOL3, TOL4, TOL5, TOL6, TOL7, TOL8, and TOL9 belong to the second group (Figure 3).

Regulators	Proteins	Yeast	Mammal	*Arabidopsis thaliana*	*Sphagnum fallax v1.1*	*Sphagnum magellanicum v1.1*	*Physcomitrella patens v3.3*	*Ceratodon purpureus GG1 v1.1*	*Ceratodon purpureus R40 v1.1*	*Marchantia polymorpha v3.1*
ESCRT-0	VPS27	1	1	0	0	0	0	0	0	0
	Hse1	1	1	0	0	0	0	0	0	0
	TOL1/2	0	4	2	3	3	2	1	1	1
	TOL3-9	0		7	4	6	2	2	1	1
ESCRT-I	VPS23	1	1	2	2	2	2	1	1	2
	VPS28	1	1	2	1	1	2	1	1	1
	VPS37	1	4	2	3	3	3	2	2	1
	MVB12	1	1	0	0	0	0	0	0	0
ESCRT-II	VPS22	1	1	1	1	1	1	1	1	1
	VPS25	1	1	1	1	1	1	1	1	1
	VPS36	1	1	1	1	1	1	1	1	1

Figure 6: ESCRT components in different species, highlighting *Arabidopsis thaliana* and *Marchantia polymorpha* (Liu et al., 2022).

This evolutionary relationship is further substantiated by phylogenetic analysis of TOL proteins from *M. polymorpha* and *A. thaliana*, as depicted in the tree topology shown in Figure 7. The phylogeny reveals a clear divergence between the two *M. polymorpha* paralogs with respect to their *Arabidopsis* counterparts: *MpTOLa* clusters within a well-supported clade together with *AtTOL1* and *AtTOL2*. In contrast, *MpTOLb* groups more closely with the remaining *Arabidopsis* paralogs, *AtTOL3* through *AtTOL9*, indicating that the two liverwort TOL homologs may have diverged early

to align with distinct subclades within the expanded *Arabidopsis* TOL gene family. This supports the hypothesis that some aspects of their functions may be evolutionarily conserved.

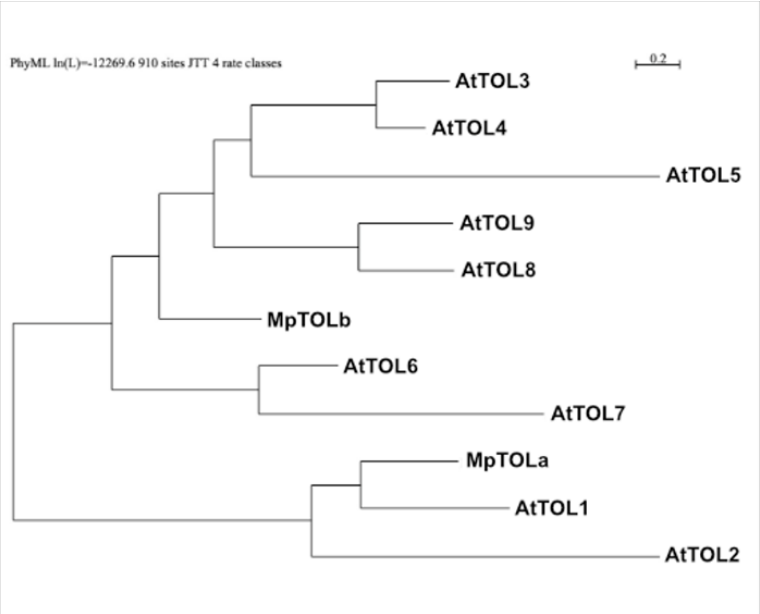


Figure 7: Maximum likelihood tree of *MpTOL* and *AtTOL* proteins. Scale bars represent the evolutionary distance of the ratio of amino acid substitutions.

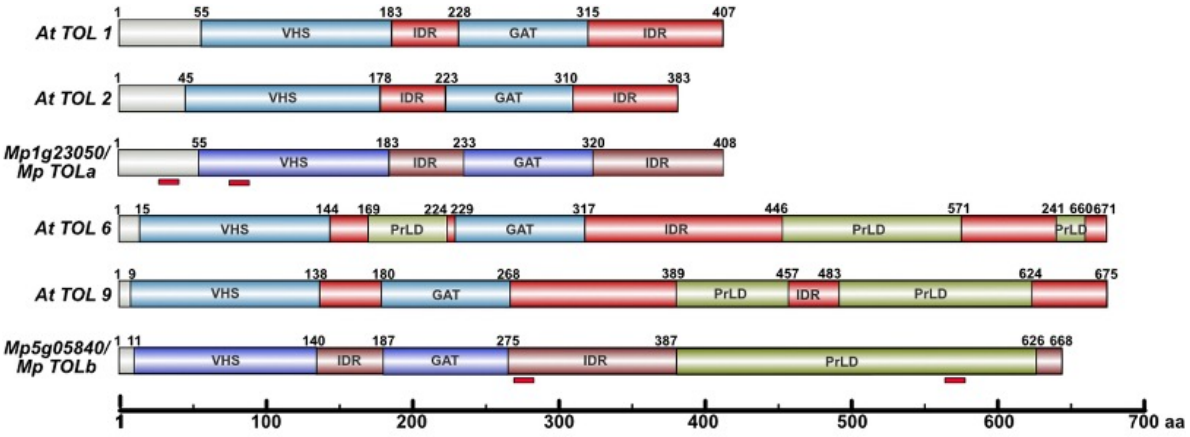


Figure 8: In silico analysis of the domain organization of the *MpTOLs* compared to their homologous *AtTOLs*. Domains: UBDs (VHS and GAT) in light-blue for *A. thaliana* and dark-blue for *M. polymorpha*, IDRs light-red for *A. thaliana* and dark-red for *M. polymorpha*, PrLD green; small red boxes beneath the sequences mark the two gRNA target sites per locus (provided by the Korbei lab).

Another interesting aspect is that *AtTOL6* and *AtTOL9* have short N-terminal domains but contain unusually extensive IDRs, which include prion-like domains (PrLDs) (Figure 8). These extensive

IDRs of TOL6 and TOL9, which contain PrLDs, represent characteristic features of proteins involved in the formation of biomolecular condensates, a cellular organization mechanism increasingly recognized as an important regulatory principle in intracellular trafficking. Furthermore, PrLDs are characterized by a high degree of conformational flexibility. This potential function makes these domains particularly relevant from a biological perspective, as they may contribute to the spatial organization of the endocytic machinery and the regulation of ubiquitinated cargo sorting (Dragwidge et al., 2024). Interestingly the *MpTOLb* also contains a long IDR containing PrLDs in its C-terminus, similar to *AtTOL6* and *AtTOL9* (Figure 8).

In *Marchantia polymorpha*, only one gene is present for each of the two groups, resulting in only two TOL proteins. *Marchantia polymorpha TOLa (Mp1g23050*) is structurally similar to *Arabidopsis thaliana TOL1* and *TOL2*, while *TOLb (Mp5g05840*) appears to share a similar domain architecture with *Arabidopsis thaliana TOL6* and *TOL9* (Figure 8).

2. AIM OF THE STUDY

The aim of this study was to investigate the roles of the two TOL proteins, TOLa and TOLb, in *Marchantia polymorpha* using CRISPR–Cas9 generated loss-of-function mutants. Based on the structural similarity between the TOL proteins of *M. polymorpha* and those of *A. thaliana*, it was hypothesized that they may also perform analogous functions within the ESCRT machinery.

Marchantia polymorpha retains only two TOL homologues, *TOLa* and TOLb, which recapitulate the domain architecture *AtTOL1/AtTOL2* and *AtTOL6/AtTOL9*, respectively. This reduced genetic redundancy, combined with the predominantly haploid life cycle of *M. polymorpha*, provides a simplified system for disceting TOL protein function, without the extensive genetic redundancy of the nine-member TOL family in *Arabidopsis thaliana*.

This raises the question of whether the structural divergence observed within TOL proteins family reflects a corresponding functional specialization. Investigating this relationship is therefore important for understanding how different TOL proteins contribute to ESCRT-mediated endosomal sorting, and for assessing the extent to which TOL function is conserved across land plants.

Objectives:

· Generate CRISPR–Cas9-mediated knockout or frameshift mutants for *tola* and *tolb* in *M. polymorph*a, resulting in premature translation termination and loss of functional protein expression.

· Characterize the resulting mutant phenotypes.

· Clone *AtTOL1, AtTOL2, AtTOL6, AtTOL9, MpTOLa,* and *MpTOLb*, to be able to test their ability to restore the wild-type phenotype in the corresponding *M. polymorpha* mutants, thereby assessing cross-species functional complementation.

3. MATERIALS AND METHODS

3.1 Materials

3.1.1 Growth Media

- Gamborg B5 Basal Medium (1/2 GB5)

Components	**Concentration**
GB5 + Vitamins	1.6 g/L

Adjust the pH to 5.6 using 1 M KOH.

For solid media add:

Components	**Concentration**
Plant agar	9 g/L

In media where mutant selection is required, the selection antibiotic must be added.
In our case, hygromycin (Hyg) was used at a final concentration of 15 mg/L.
Additionally, cefotaxime (Cef) can be added at a final concentration of 50 mg/L to prevent unwanted agrobacterial contamination.

- Gamborg B5 Basal sup Medium (1/2 GB5 sup)

Components	**Concentration/Volume**
Gamborg B5 Basal Medium (1/2 GB5)	500 mL
Sucrose	5%
Acetosyringone	100 µM

- Luria-Bertani (LB)

Components	**Concentration**
Peptone	10 g/L

Yeast extract	5 g/L
NaCl	10 g/L

Adjust the pH to 7.0 with NaOH 10 M.

For solid media, add 1.5% Bacto agar. In addition, when preparing selective solid LB media, the appropriate selection antibiotic must be included; in our case, 50 mg/L of Spectinomycin (Spec), 50 mg/L of Ampicillin (Amp), 50 mg/L of Rifampicin (Rif), 50 mg/L of Kanamycin (Kan) or 50 mg/L of Gentamicin (Gent).

For all media, the powdered components were first dissolved in water, the pH was adjusted if necessary. The media were then distributed into Schott bottles already with or without agar, and subsequently sterilized by autoclaving. Antibiotics were added under sterile conditions after autoclaving, once the medium had cooled sufficiently to avoid heat-induced antibiotic inactivation.

3.1.2 Solutions and Buffers

- 2X CTAB

Components	**Concentration**
Cetyl trimethylammonium bromide	2% w/v
1 M Tris/HCl pH 8.0	100 mM (100 mL/L)
0.5 M EDTA pH 8.0	20 mM
NaCl	0.818 g/L
Polyvinyl pyrrolidone (PVP)	1% w/v

- 1 M Tris/HCl pH 8.0

Components	**Concentration**
Tris (2-amino-2-hydroxymethyl-1,3-propanediol)	212.2 g/L

Adjust the pH to 8.0 using concentrated HCl.

- 0,5 M EDTA pH 8.0

Components	**Concentration**
$Na_2EDTA \bullet 2\ H_2O$	186.12 g/L

Bring to pH 8.0 using 10 M NaOH.

- 1 M KOH

Components	**Concentration**
KOH	70 g/L

- 10 M NaOH

Components	**Concentration**
NaOH	500 g/L

The dissolution of NaOH and KOH in H_2O is a highly exothermic reaction.
The solutions must be prepared with extreme care in plastic beakers and NaOH or KOH needs to be slowly added under continuously stringing.

- 70% Glycerol

Components	**Concentration**
Glycerol 100%	700 mL/L

- 10% Glycerol

Components	**Concentration**
100% Glycerol	100 mL/L

- TE buffer

Components	**Concentration**
1 M Tris/HCl pH 8.0	10 mM
0.5 M EDTA pH 8.0	1 mM

- 50x TAE buffeer

Components	**Concentration**
TRIS	242.28 g/L
Acetic acid	51.1 mM
0.5 M EDTA pH 8.0	100 mM

All these solutions need to be autoclaved and after that they can be stored at room temperature.

- Sterilizing solution

Dissolve 1 milton antibacterial tablet (Milton Baby Sterilising Tablets Antibacterial Cleaner) in 1 L of previously autoclaved ddH_2O.

Store up to 3 months at 4 °C.

- 100 mM IPTG stock

236 mg of Isopropyl-β-D-thiogalactopyranoside were dissolved in 10 mL ddH2O.

- X-Gal stock

600 mg of 5-Bromo-4-Chloro-3-Indolyl β-D-Galactopyranoside were dissolved in 10 mL ddH2O.

- Blue/white selection mixture

25 µL X-Gal, 25 µL IPTG, and 25 µL ddH2O were mixed together.

3.1.3 Plasmids used

Name	Size (bp)	Resistance in Bacteria	Resistance in plants
pGEM T	3.000	Ampicillin	-
pH7FWG2	12.303	Spectinomycin	Hygromycin
pMpGE010	17.689	Spectinomycin	Hygromycin

Table 1: *list of the plasmid used in the study.*

3.1.4 Bacterial strains used

Microrganism	Strain name	Genotype	Reference
Escherichia coli	DH5α	F– φ80lacZΔ M15 Δ (lacZYA-argF) U169 recA1 endA1 hsdR17 (rK– mK+) phoA supE44 λ- thi–1 gyrA96 relA1	Grant et al., 1990
Escherichia coli	ccdB survival	F-*mcr*A Δ(*mrr*-*hsd*RMS-*mcr*BC) φ80*lac*ZΔM15 Δ*lac*X74 *rec*A1 *ara*Δ1 39 Δ(*ara*- *leu*) 7697 *gal*U *gal*K *rps*L(Str^R) *end*A1 *nup*G *fhu*A::*IS2*	Korbei Lab
Agrobacterium tumefaciens	GV3101	C58 (RifR) pMP90 (pTiC58DT-DNA) (GentR) Nopaline	Koncz and Schell, 1986

Table 2: *list of the bacterial strain used in the study.*

3.2 Plant Methods

3.2.1 Growth Conditions of *Marchantia polymorpha*

Marchantia polymorpha plants were grown in a growth chamber under controlled environmental conditions at 22 °C.

For vegetative (asexual) growth, plants were maintained on shelves illuminated with white light.

To induce sexual development red light is necessary, 14-day-old plants were transferred to specific light conditions consisting of white light and far-red light.

3.2.2 Agrobacterium-mediated Transformation of *Marchantia polymorpha*

The procedure started with dried mature *M. polymorpha* sporangia, which were crushed with a sterile spatula in sterile ddH_2O. The resulting suspension was filtered through a 40 μm cell strainer to collect the spores. The filtrate was then divided into 1.5 mL microcentrifuge tubes and centrifuged at room temperature for 1 min at 12,000–13,000 rpm.

The supernatant was discarded, the pellet was resuspended in Milton sterilizing solution, and the suspension was incubated for 20 min with gentle inversion every 2–3 min.

After incubation, the samples were centrifuged again and the supernatant was discarded. The spores were washed three times with sterile water, centrifuging each time at 10,000–13,000 rpm for 1 min.

After the final wash, 100 μL of the spore suspension was spread onto 1/2 GB5 medium in a Petri dish using a sterile Drigalski metal spatula. Once the plates were completely dry, they were sealed with masking tape and incubated upside down at 22 °C for 7 days. After 7 days, the thalli were fully developed and were either used immediately or stored at 4 °C for up to 1 week.

Once the thalli had developed, the transformation procedure was performed. A single colony of transformed *Agrobacterium tumefaciens* was inoculated into liquid medium supplemented with the appropriate antibiotics and incubated overnight at 28 °C in a shaking incubator (150–200 rpm). When the culture reached an OD_{600} of 0.4–0.5, it was centrifuged at 5,000 rpm for 5 min at room temperature. The supernatant was discarded, and the bacterial pellet was resuspended in 1/2 GB5 liquid medium supplemented with sucrose and acetosyringone to a final OD_{600} of 0.5. The culture

was protected from light by covering it with aluminum foil and incubated at 28 °C with shaking (200 rpm) for 6 h.

Towards the end of the 6 h incubation, the 7-day-old *M. polymorpha* thalli were collected from the plates. Using a sterile spatula and 1/2 GB5 liquid medium, the thalli were gently scraped from the surface of the solid medium, resuspended in the liquid medium using a micropipette, and transferred to a sterile glass flask covered with aluminum foil.

After the 6 h incubation, 50 µL of the *A. tumefaciens* suspension was added directly to the flask containing the thalli for each plasmid. Two plasmid combinations were used, resulting in two independent transformation experiments.

The co-cultures were incubated under a 12 h light/12 h dark photoperiod with gentle shaking for 2–3 days. The dark period was maintained because continuous light can inhibit the growth of *A. tumefaciens*.

After 2 days of co-cultivation, each transformation was filtered to maximize recovery of the plant material. The retained material was washed several times with sterile water, followed by a final wash with sterile ddH_2O supplemented with cefotaxime to eliminate residual *A. tumefaciens*. The recovered material was transferred to a 50 mL centrifuge tube containing sterile water and cefotaxime and gently resuspended by pipetting up and down. An aliquot of 900–2,000 µL of the suspension was then spread onto each 1/2 GB5 plate supplemented with the appropriate selective antibiotic. The plates were incubated in the *Marchantia* growth chamber without being inverted.

After approximately 2 weeks, the transformed plants were transferred onto fresh 1/2 GB5 medium containing the selective antibiotic.

The original selection plates were stored at 4 °C for up to 6 weeks and periodically exposed to light to maintain plant viability.

3.2.3 Transfer of *Marchantia polymorpha* to Soil

To allow the continued cultivation of *Marchantia polymorpha* plants affected by fungal contamination of the culture medium, contaminated plants were transferred from agar plates to soil.

The soil routinely used for *M. polymorpha* cultivation in the laboratory was prepared using the freeze–thaw method and was not subjected to any additional treatment before plant transfer.

The soil was thoroughly moistened with tap water. Plants were carefully removed from the agar medium using sterile tweezers, avoiding damage to the thalli and rhizoids. The plants were then placed directly onto the surface of the soil and gently positioned to ensure contact with the substrate. Plants were maintained under the same growth conditions used for vegetative cultivation and monitored for further development and fungal growth.

3.2.4 Gemmae Sterilisation

Once the plants had grown in soil, gemmae were collected for re-establishment under sterile in vitro culture. Gemmae were harvested from the gemma cups and transferred into a 1.5 mL microcentrifuge tube containing a Milton disinfectant solution prepared in sterile distilled water.
After incubation for 20 min at room temperature, the gemmae were transferred onto 1/2 GB5 medium supplemented with the appropriate selective antibiotic when required (hygromycin).

3.2.5 *Marchantia polymorpha* Gemmae Propagation

To maintain *Marchantia polymorpha* cultures, plants were propagated every 4–6 weeks using gemmae.
Gemmae were collected from gemma cups using sterile tweezers or sterile pipette tips and individually transferred onto fresh 1/2 GB5 medium. During the initial establishment of mutant lines, hygromycin was used for selection to facilitate the identification and maintenance of transformed plants. Once the mutant lines had been successfully established and confirmed, gemmae were propagated on 1/2 GB5 medium without antibiotic selection. Once the mutant lines had been established and confirmed, gemmae were propagated on 1/2 GB5 medium without antibiotic selection. Wild-type plants were also propagated on 1/2 GB5 medium without antibiotics.
Four or five gemmae were placed on each Petri dish. When five gemmae were transferred, four were positioned near the edges of the plate to form a square, with the fifth placed in the center.

3.2.6 Plant Genomic DNA Extraction Using the CTAB Method

Plant genomic DNA was extracted from approximately 1–2 cm of *M. polymorpha* thallus tissue using the CTAB method. Plant material was collected in 2 mL tubes containing metal beads, snap-frozen in liquid nitrogen, and homogenised using a Retsch MM200 homogeniser at 25 s^{-1} for 1 min 20 s.

Following homogenisation, 200 µL of 2× CTAB buffer was added to each sample. Samples were incubated at 65 °C for 5 min and subsequently mixed with 200 µL chloroform by vortexing. Samples were centrifuged at 15,400 rpm for 10 min at room temperature, and the upper aqueous phase was transferred to a new tube.

Genomic DNA was precipitated by adding 2.5 volumes of absolute ethanol and incubating the samples at −20 °C for at least 20 min or overnight. Samples were then centrifuged at 15,400 rpm for 15 min at 4 °C. The supernatant was discarded, and the DNA pellet was washed with cold 70% ethanol. After a second centrifugation, the supernatant was removed and the pellet was air-dried at 37 °C.

The DNA pellet was resuspended in 45 µL TE buffer (pH 8.0) and incubated at 37 °C for 15 min. Extracted genomic DNA was stored at −20 °C until further use.

3.3 Bacterial Methods

3.3.1 Preparation of *Agrobacterium tumefaciens* (or *Escherichia coli*) Electrocompetent Cells

First, a small amount of *Agrobacterium tumefaciens* strain GV3101 was taken from a glycerol stock stored at −70 °C using a sterile loop and streaked onto a plate containing the appropriate selective antibiotics (rifampicin and gentamicin). The plate was incubated upside-down at 28 °C for 48h.

After the incubation, a single colony was picked and inoculated into 10 mL of liquid LB medium supplemented with antibiotics in an Erlenmeyer flask, and grown for 24 h at 28 °C with shaking at 200 rpm (starting culture).

On the next day, the OD_{600} of the culture was measured. When it reached 1.5–3.0, an appropriate volume of the starting culture was used to inoculate 500 mL of LB medium to a starting OD_{600} of 0.01. The culture was incubated overnight at 28 °C with shaking at 200 rpm.

The following day, when the OD_{600} reached approximately 0.5–0.7, the culture was placed on ice for 1 h. Cells were then harvested by centrifugation at 5000 × g for 15 min at 4 °C.

The cells were subsequently washed as follows:

- First wash: the pellet was resuspended in 400 mL of sterile, cold distilled water and centrifuged at 5000 × g for 15 min at 4 °C.
- Second wash: the pellet was resuspended in 200 mL of sterile, cold distilled water and centrifuged under the same conditions.
- Third wash: the pellet was resuspended in 20 mL of sterile, cold 10% glycerol and centrifuged at 5000 × g for 15 min at 4 °C.
- Final resuspension: the pellet was resuspended in 2 mL of sterile, cold 10% glycerol. The suspension was then aliquoted (50 µL per tube), snap-frozen in liquid nitrogen, and stored at −70°C.

This protocol can also be applied for the preparation of electrocompetent *E. coli* cells, with some modifications: no antibiotics are required for the DH5α strain, *E. coli* cultures are grown at 37 °C and the incubation times are overnight (approximately 16h). Since E. coli grows faster than *A. tumefaciens* the inoculation of the 500 ml culture is done in the morning of the preparation day.

3.3.2 Electroporation into Competent *A. tumefaciens* (or *E. coli*) cells

For DNA transformation by electroporation into *A. tumefaciens* or *E. coli* cells, a frozen aliquot of electrocompetent cells was first thawed on ice. Subsequently, 1–3 µL of DNA was added to the cells and gently mixed, avoiding the formation of air bubbles. The mixture was then transferred into a pre-chilled sterile electroporation cuvette.

Electroporation was performed using a Bio-Rad MicroPulser by applying an electric pulse. For *E. coli*, a voltage range of 200–300 V (with 10 V precision) was used, according to the manufacturer's recommendations.

Cold conditions were maintained throughout the procedure.

Immediately after electroporation, the cells were transferred into a microcentrifuge tube and supplemented with liquid LB medium. The cells were then incubated for 1 h at 37 °C for *E. coli* or at 28 °C for *A. tumefaciens* to allow recovery.

Finally, the cells were plated onto LB agar plates containing the appropriate selection antibiotics.

3.3.3 Heat Shock Transformation of *E. coli*

Under sterile conditions, 100 µL of competent cells was mixed with 1–2 µL of plasmid DNA. The mixture was incubated on ice for 10 min and then transferred to an Eppendorf 5436 Thermomixer preheated to 42 °C for 90 s. Immediately after the heat shock, the cells were returned to ice.

This thermal shock transiently increases the permeability of the bacterial membrane, facilitating the uptake of plasmid DNA.

Next, 400 µL of LB medium was added, and the cells were incubated at 37 °C for 40–60 min to allow recovery and expression of the plasmid-encoded antibiotic resistance gene.

Finally, the transformed cells were plated onto LB agar plates supplemented with the appropriate selective antibiotic. To obtain well-isolated colonies, the transformation mixture was divided between two plates: one plate received approximately one-tenth (1:10) of the total volume, while the second plate received the remaining nine-tenths (9:10).

3.3.4 Plasmid DNA Extraction

For plasmid DNA extraction, *E. coli* cells containing the plasmid of interest were first grown in liquid LB medium supplemented with the appropriate antibiotic. A single bacterial colony was inoculated into 5 mL LB medium and incubated at 37 °C for approximately 16 h with shaking at 180 rpm. Following incubation, the bacterial culture was centrifuged to collect the cells, and the supernatant was discarded.

Plasmid DNA was then extracted from the bacterial pellet using a commercial miniprep kit, according to the manufacturer's instructions.

3.3.5 Blue/White Screening of Positive Clones

Blue/white screening was performed to identify recombinant colonies carrying inserts within the LacZ-containing T/A vector. Before plating the transformed bacterial culture, 75 µL of a blue/white screening solution, consisting of sterile water, IPTG, and X-Gal, was evenly spread onto the surface of selective LB agar plates. The plates were then allowed to dry under sterile conditions next to a Bunsen burner.

The transformed bacterial culture was subsequently divided, and 1/10 and 9/10 of the transformation mixture were plated onto the prepared plates. The plates were incubated overnight at 37 °C. Following incubation, white colonies were considered putative recombinant clones, whereas blue colonies were considered to contain the empty vector.

3.3.6 Glycerol Stock Preparation

Bacterial strains were grown overnight in liquid LB medium under the appropriate antibiotic selection. Under sterile conditions, 1 mL of the overnight bacterial culture was mixed with 1 mL of sterile 70% glycerol. The resulting glycerol stocks were stored at −70 °C.

3.4 Molecular Biology Methods

3.4.1 PCR

PCR amplification was performed using different DNA polymerases depending on the application. For genotyping, FIREPol Master Mix Ready to Load (5x) was used because of its robustness and low cost, making it suitable for routine PCR. For cloning, Q5 High-Fidelity DNA Polymerase (NEB) was used because of its proofreading activity and high fidelity, reducing the probability of introducing PCR-induced mutations into the amplified DNA fragments.
For the TA-cloning of the *MpEF1ap* promoter into the pGEM-T vector, ALLin™ RPH Polymerase was used because it generates PCR products with 3′-A overhangs, which are compatible with the T-overhangs of the pGEM-T vector.

A PCR requires several components to work properly: ddH_2O, Polymerase, Polymerase buffer, DNA, $MgCl_2$, dNTPs, Primer Forward, Primer Reverse
The final reaction volumes and reagent concentrations varied depending on the DNA polymerase used and the purpose of the PCR.

When the FIREPol® Master Mix Ready to Load (5×) polymerase was used, the reaction mixture contained the polymerase, loading dye, reaction buffer, $MgCl_2$, and dNTPs already included in the master mix. The composition of the reaction mixture is reported in Table 3.

Components	Initial concentration	Final concentration	µL needed in final volume 10 µL	µL needed in final volume 50 µL
ddH2O			5	25
Primer Forward	2 µM	0.2 µM	1	5
Primer Reverse	2 µM	0.2 µM	1	5
DNA			1	5
FIREPol® Master Mix Ready to Load	5X	1X	2	10

Table 3: *Composition of the PCR reaction using FIREPol® Master Mix Ready to Load (5×) polymerase.*

When ALLin™ RPH Polymerase was used, PCR reactions were prepared in a final volume of 50 µL according to the manufacturer's instructions. The composition of the reaction mixture is reported in Table 4.

Components	Initial concentration	Final concentration	µL needed in final volume 50 µL
ddH2O			34.4
Primer Forward	10 µM	0.4 µM	2
Primer Reverse	10 µM	0.4 µM	2
DNA			1
Polymerase	5 U/µL	0.06 U/µL	0.6
Buffer 5X	5X	1X	10

Table 4: *Composition of the PCR reaction using ALLin™ RPH polymerase.*

When Q5 High-Fidelity DNA Polymerase (NEB) was used, PCR reactions were prepared in a final volume of 50 µL according to the manufacturer's instructions. The composition of the reaction mixture is reported in Table 5.

Components	Initial concentration	Final concentration	µL needed in final volume 50 µL
ddH2O			32.5
Buffer 5X	5X	1X	10
Primer Forward	10 µM	0.5 µM	2.5
Primer Reverse	10 µM	0.5 µM	2.5
dNTPs	10 mM	200 µM	1
DNA			1
Polymerase	2 U/µL	0.02 U/µL	0.5

Table 5: Composition of the PCR reaction using Q5® High-Fidelity DNA Polymerase.

When required, gradient PCR was performed using different annealing temperatures to determine suitable conditions for primer amplification.

For colony PCR, individual bacterial colonies were directly transferred into the PCR reaction mixture using a sterile pipette tip. No prior DNA extraction was performed.

3.4.2 List of Primers Used

Name	Sequence
Male-Seq-F	5’ -CCAAGTGCGGGCAGAATCAAGT- 3’
Male-Seq-R	5’ -TTCATCGCCCGCTATCACCTTC- 3’
Female-F	5’ -GACGACGAAGATGTGGATGAC- 3’
Female-R	5’ -GAAACTTGGCCGTGTGACTGA- 3’
Mp1g-PCR-F	5’ -GGTTTGGTGGGAGAGAGCTTGACTG- 3’
Mp1g-PCR-R	5’ -ATTGGAGGTGAAGGTGCGATTGAC- 3’
Mp5g-PCR-F	5’ -TTCGGTTCTCATTCATCTCCATAG- 3’
Mp5g-PCR-F2	5’ -AACCTAGTCAGCGTGAGATG- 3’
Mp5g-PCR-R	5’ -GGGAAAGGGTGAAGCTTGCTGTTG- 3’
Mp5g-PCR-R2	5’ -TTGTCCACCAAGGGCCTGATT- 3’
Mp5g-PCR-R3	5’ -ACTCAGATCCACCAAGTCTC- 3’
MpEF1a_HR_F	5’ -TGATCCAAGCTCAAGCT**AAGCTT**CAAATGAGTCACACACATTGTTGA- 3’
MpEF1a_HR_R	5’ -GCCCTTGCTCACCAT**ACTAGT**CAACCTTTCTGCAGGCACAT- 3’
MpEF1ap-seq-F	5’ -CGGTAAGGTGTTCAGTTCGG- 3’
Hyg-F	5’ -CAATGACCGCGTTATGCGG- 3’
Hyg-R	5’ -CTCGGAGGGCGAAGAATCTC- 3’
Kan_f-n	5’ -AAGGCGATAGAAGGCGATGC- 3’
Kan_r-n	5’ -GATGGATTGCACGCAGGTTC- 3’
T35s-r	5’ -GGAACTACTCACACATTATTCTGG- 3’
RB T-DNA-seqf	5’ -TACAAATGGACGAACGGATAAACC- 3’
TOL1-RT-F1	5’ - CCAGTGAACTTCGCTACCTACC- 3’
TOL2seq-F	5’ -GGTCTTGACTATAACTTTGGGAAC - 3’
TOL6q-F	5’ -ACCAGTGAGTCATCCACCGT- 3’
TOL9T-f	5’ -GAACTGTGGTGACATGGTTC- 3’
XFP-u	5’ -ATAGATAGCATCACTA- 3’
p35S-f	5’ -GACCAAAGGGCTATTGAGAC- 3’

Table 6: *list of primers used in this study. The SpeI and HindIII cleavage sites are underlined and in bold.*

3.4.3 Agarose Gel Electrophoresis

Agarose gel electrophoresis is a technique used to separate DNA fragments based on their size, measured in base pairs (bp).

Once the DNA is loaded onto the agarose gel, it is subjected to an electric field, and the DNA fragments, which are negatively charged, migrate toward the positive pole at different speeds depending on the length of the fragment. Smaller fragments migrate faster than larger ones, as they can more easily pass through the agarose matrix.

Agarose gels were prepared at concentrations of 0.8% or 1% (w/v) by dissolving 1.2 g or 1.5 g agarose, respectively, in 150 mL 1× TAE buffer. The solution was heated in a microwave at 700 W for approximately 3 min until completely dissolved and then cooled to approximately 55 °C. After cooling, 7.5 µL peqGREEN dye was added and mixed thoroughly. The gel was then poured into a casting tray and allowed to solidify for approximately 30 min.

DNA samples were mixed with loading buffer and loaded onto the gel together with 5 µL GeneRuler 1 kb DNA Ladder for fragment size estimation. Electrophoresis was performed in 1× TAE buffer at 130 V for 25 min. DNA bands were visualized using a GelDoc Imaging System under UV illumination.

Agarose gel electrophoresis was performed after PCR amplification and, when required, following enzymatic digestion to assess the presence and approximate size of the resulting DNA fragments.

3.4.4 DNA Purification

DNA purification, including purification of PCR products, was performed using the Monarch® PCR & DNA Cleanup Kit (NEB), according to the manufacturer's instructions.

3.4.5 DNA Gel Extraction

Gels were visualized using a UV transilluminator and DNA bands were identified by comparison with a DNA ladder to determine fragment size. Gel slices containing the desired DNA fragments were carefully excised using a clean scalpel while minimizing the amount of surrounding agarose.

The excised gel pieces were transferred into pre-weighed 1.5 mL tubes and immediately processed for DNA purification using the Monarch DNA Gel Extraction Kit (NEB), according to the manufacturer's instructions.

3.4.6 DNA Quantification

DNA concentration was measured using a NanoPhotometer.

All samples were measured at wavelengths of 260 and 280 nm simultaneously, with baseline correction at 340 nm. Before each measurement and at the end, the pedestal was cleaned with a precision wipe moistened with ddH_2O.

For each solution to be measured, 1 µL was pipetted onto the pedestal and the arm was closed gently. The buffer, which was used to elute DNA, was measured as blank solution before measuring the DNA solution.

A DNA sample with an absorbance ratio (260/280 nm) of about 1.9 was considered pure.

3.4.7 Restriction Enzyme Digestion

Restriction enzymes possess the ability to catalyze the cleavage and degradation of nucleic acids through the hydrolysis of phosphodiester bonds. These enzymes produce internal cuts in DNA, specifically at defined DNA recognition sequences.

By using restriction enzymes, it was primarily possible to generate cohesive ends on the DNA double helix at specific sites, thereby facilitating the subsequent ligation of these ends.

Furthermore, they proved repeatedly useful for verifying the correctness of various experimental processes.

Components	**Volume (µL)**
Sterile ddH2O	Variable
Buffer (10x)	5
Restriction enzyme	5

Plasmid DNA (target amount 5 µg)	Variable

Table 7: *Reaction components used for DNA cleavage.*

For double restriction enzyme digestions, 2–3 µL of each restriction enzyme was used.
The reaction mixture was incubated at 37 °C for 3 hours, followed by heat inactivation at 65 °C for 15 min to terminate the enzymatic activity.

3.4.8 Ligation

Ligation is the process of joining two complementary DNA ends previously generated by restriction enzyme digestion. This reaction is catalyzed by T4 DNA ligase, which, in the presence of a ligation buffer containing ATP, catalyzes the formation of phosphodiester bonds between adjacent nucleotides.
The insert and vector were ligated at an insert-to-vector molar ratio of 3:1, calculated using the following formula:

$$\text{ng (vector)} \times \left(\frac{\text{bp (insert)}}{\text{bp (vector)}} \right) \times 3$$

Components	**Volume (µL)**
Sterile ddH2O	Variable
Ligase Buffer (2x)	5
Vector variable	Variable
Insert variable	Variable
T4 Ligase	1

Table 8: *Composition of a 10 µL DNA ligation mixture.*

The reaction mixture was first incubated for 1 h at room temperature, followed by an overnight incubation at 16 °C. On the following day, the reaction was inactivated by heating the sample at 65 °C for 15 min.

3.4.9 Gateway Cloning: LR Reaction

Gateway cloning is a recombination-based cloning system that enables the efficient transfer of a DNA fragment between different plasmid vectors without the use of restriction enzymes or DNA ligase. The system is based on site-specific recombination between compatible *att* recombination sites derived from bacteriophage λ.

In the LR reaction, the DNA fragment of interest, previously cloned into an entry vector and flanked by *attL* sites, is recombined with a destination vector containing compatible *attR* sites. The reaction is catalyzed by the LR Clonase™ enzyme mix, which mediates site-specific recombination, generating an expression clone in which the insert is transferred into the destination vector. During the LR reaction, the *ccdB* cassette in the destination vector is replaced by the DNA insert. Non-recombined destination vectors retain the toxic *ccdB* gene and are therefore not propagated in standard *E. coli* strains.

The resulting expression vector was subsequently transformed into competent *E. coli* cells for plasmid amplification.

Components	**Volume needed for a 10 µL reaction**
Entry clone	1-7 µL (50-150 ng)
Destination vector	1 µL (150 ng/µL)
Clonase	1 µL
TE buffer	To 10 µL

Table 9: *Reaction components used for LR reaction.*

3.4.10 DNA Sample Preparation for Sanger Sequencing

Before Sanger sequencing, the DNA region of interest was amplified by PCR in a 50 µL reaction using the FIREPol® Master Mix Ready to Load (5×). For plasmid sequencing, plasmid DNA was extracted as described above.

DNA concentrations were measured using a NanoPhotometer, and PCR products were prepared according to the requirements of the sequencing provider.

For Sanger sequencing of PCR products, 12 µL of purified PCR product was prepared at a concentration appropriate for the size of the amplified fragment, as reported in Table 10.

Length of the fragment	**Concentration needed**
100 - 400 bp	2 - 6 ng/µL
401 - 900 bp	4 - 17 ng/µL
901 - 2000 bp	12 - 70 ng/µL

Table 10: *Required DNA concentration according to the size of the amplified fragment for Sanger sequencing.*

For plasmid sequencing, plasmid DNA was prepared at a concentration of 80 ng/µL. A total volume of 15 µL was submitted, consisting of 12 µL of plasmid DNA and 3 µL of the corresponding sequencing primer at a concentration of 20 µM.

4. RESULTS AND DISCUSSION

4.1 CRISPR/Cas9-mediated generation of *MpTOLa* and *MpTOLb* mutant candidates

To investigate the roles of MpTOLa and MpTOLb in *M. polymorpha*, a CRISPR/Cas9-based approach was used to target the *MpTOLa* and *MpTOLb* loci. Four CRISPR/Cas9 expression vectors were used, with two vectors designed for each locus. Each vector carried a gene-specific guide RNA (gRNA) targeting a distinct sequence within the corresponding locus (Figure 10). The two gRNAs targeting the same gene were used together to introduce two Cas9-mediated cuts within the locus, with the aim of generating a deletion between the two target sites that could result in a gene knockout or other mutations affecting protein function.

The CRISPR/Cas9 constructs had been generated prior to the beginning of the present work according to the genome-editing strategy established for *M. polymorpha* by Sugano et al. (2018). Briefly, the gRNA sequences had been previously cloned independently into the binary vector pMpGE_En03, which provides the gRNA expression cassette (Figure 9). The resulting gRNA-containing constructs were subsequently transferred into the binary vector pMpGE010 by Gateway recombination, generating the final CRISPR/Cas9 expression vectors used for *M. polymorpha* transformation.

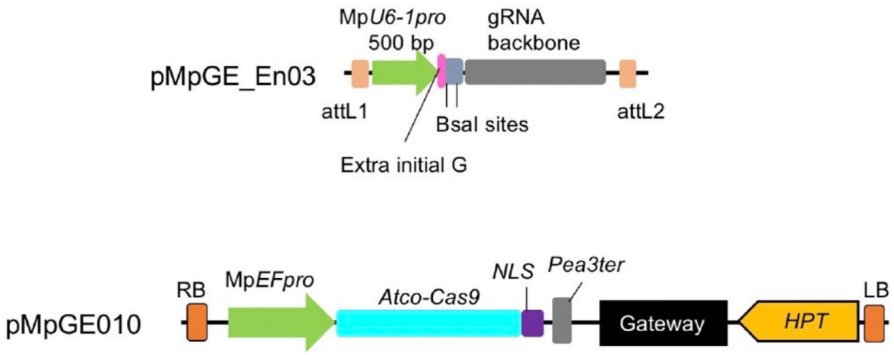


Figure 9: Design of the Gateway-based all-in-one binary vector pMpGE010 and the entry plasmid pMpGE_En03 used for gRNA cloning. pMpGE010 contains a cassette for the expression of *Arabidopsis thaliana* codon-optimized Cas9 (Atco-Cas9) fused to a nuclear localization signal (NLS) under the control of the *M. polymorpha* EF promoter (MpEFpro), a Gateway cassette, and a hygromycin phosphotransferase (HPT) resistance cassette. pMpGE_En03 contains two BsaI recognition sites upstream of the gRNA backbone for the insertion of the guide sequence by ligation,

with or without an additional initial G. gRNA expression is driven by a 500-bp fragment of the *M. polymorpha* U6-1 promoter (MpU6-1pro) (Sugano et al., 2018).

The final CRISPR/Cas9 vectors therefore contained the components required for genome editing, including the Cas9 expression cassette, the gene-specific gRNA cassette targeting either the *MpTOLa* or *MpTOLb* locus and driven by a 500-bp fragment of the ubiquitously expressed *M. polymorpha* U6-1 promoter (MpU6-1pro), and the HPT selection marker. Since these constructs were already available at the beginning of the present study, no vector construction was performed as part of this work.

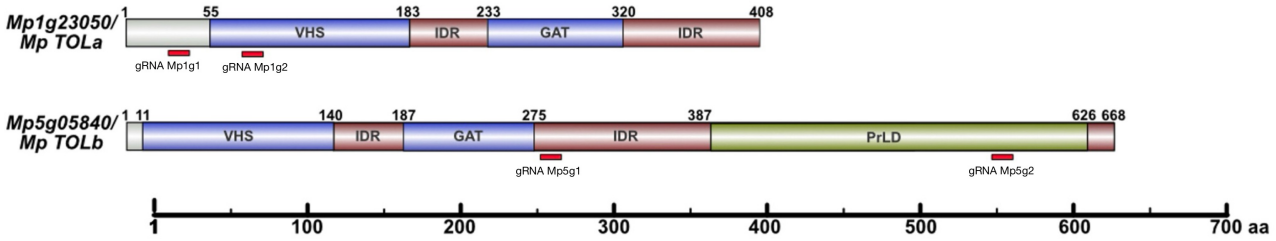


Figure 10: Genomic localization of the two gRNA target sites within *MpTOLa* (*Mp1g23050*) and *MpTOLb* (*Mp5g05840*).

The four CRISPR/Cas9 vectors were then individually introduced into electrocompetent *Agrobacterium tumefaciens* cells by electroporation. The resulting *A. tumefaciens* strains were subsequently used for transformation of one-week-old *M. polymorpha* thalli.

For each transformation, the two constructs targeting the same locus were used together.
The vectors carrying gRNA Mp1g1 and Mp1g2 were combined to target the *MpTOLa* locus, whereas the vectors carrying gRNA Mp5g1 and Mp5g2 were combined to target the *MpTOLb* locus (Figure 10).

4.2 Selection and molecular characterization of putative *M. polymorpha MpTOLa* and *MpTOLb* mutant lines

Following transformation, the plant material was plated on selective medium containing hygromycin (Hyg). Since all four CRISPR/Cas9 vectors carried the same resistance marker, Hyg

selection allowed transformed plants to be distinguished from non-transformed plants, but did not allow discrimination between plants carrying one or both of the two gRNA-containing constructs targeting the same locus.

To identify plants carrying both constructs, the transformed plants were first transferred to fresh selective medium 17 days after transformation and subsequently screened. In total, 168 plants were transferred and grouped according to their size, based on their growth during the preceding 17 days. This grouping facilitated subsequent monitoring of development and phenotypic comparison among plants at similar developmental stages. The original transformation plates were maintained at 4 °C as a backup source of plant material, allowing additional plants to be recovered if required.

Once the plants had reached a suitable size, genomic DNA was extracted using the CTAB method for subsequent genotyping.

4.2.1 Molecular screening of the *MpTOLa* locus

The *MpTOLa* locus was amplified using the primer pair Mp1g-PCR-F and Mp1g-PCR-R. The resulting PCR products were analysed by agarose gel electrophoresis and compared with the corresponding wild type (WT) amplicons. The expected WT amplicon was 893 bp, whereas simultaneous cleavage at the two gRNA target sites was expected to generate a shorter amplicon of 599 bp.

Among the plants analysed, plant 43 displayed two distinct bands. One faint band migrated at approximately the same position as the WT amplicon. The second, more intense band, was observed at approximately 600 bp. The size of the shorter product was consistent with the large deletion expected from simultaneous cleavage at the two gRNA target sites, identifying plant 43 as a candidate for further molecular characterization.

Sequencing of the PCR product from plant 43, however, revealed an anomalous sequence pattern. The sequence was identical to the expected reference sequence at positions 1–84, 356–586, and from position 1227 onwards. In addition, a duplicated sequence corresponding to positions 359–614 and a deletion within the targeted region were detected. The origin of this pattern could not be determined. One possible explanation was the presence of genetically distinct cell populations within the plant, consistent with a possible chimeric state. However, this hypothesis could not be experimentally confirmed.

The plant also displayed a distinct phenotype compared with WT plants of the same age (Figure 11). Plant 43 at approximately 40 days after transformation was already smaller than the WT controls. As the plant continued to grow, additional morphological differences became apparent.

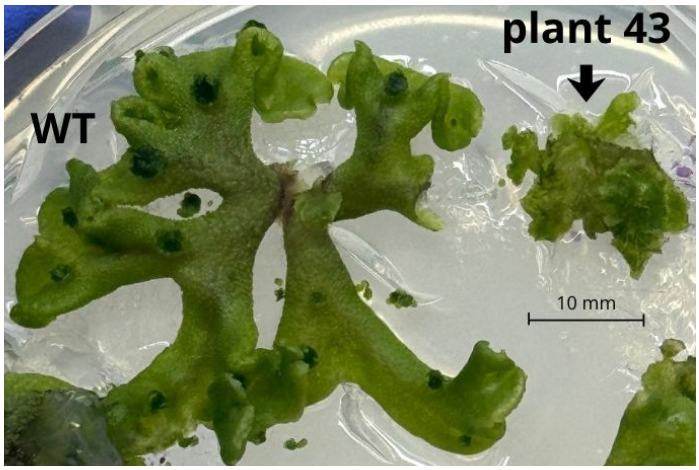


Figure 11: Representative image of plant 43, indicated by the black arrow, compared with WT plants of the same age (approximately 40 days).

In addition to its reduced size, at day 63 after transformation, the thallus showed an asymmetric morphology. One side exhibited a morphology comparable to that of WT plants, whereas the opposite side appeared more compact and vertically oriented, with reduced lateral expansion and more pronounced longitudinal growth (Figure 12). Thus, the asymmetry was not clearly evident at the earlier time point shown in Figure 11, but became apparent as the plant developed further.

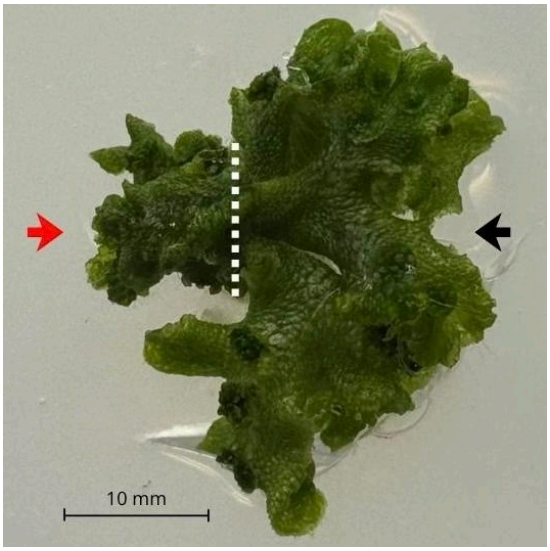


Figure 12: Representative image of plant 43, at day 63 after transformation, showing the asymmetric thallus morphology. The dotted white line indicates the approximate axial division of the thallus. The red arrow indicates the morphologically altered region, whereas the black arrow indicates the region showing a morphology comparable to WT.

To determine whether this phenotype was maintained upon vegetative propagation, gemmae were collected separately from the WT-like and morphologically altered regions of the thallus and propagated independently. Gemmae originating from the WT-like region developed into plants phenotypically comparable to WT, whereas those originating from the altered region reproduced the abnormal phenotype. This correspondence suggested that the phenotype was associated with the tissue from which the gemmae originated.

However, sequencing of the propagated plants revealed sequences identical to the WT reference. This indicated that the sequence alteration detected in plant 43 was not stably maintained upon vegetative propagation. Thus, although the abnormal phenotype was reproducible, a stable CRISPR/Cas9-induced genetic alteration could not be established as its cause. Nevertheless, the phenotype of plant 43 was used as a preliminary criterion for the selection of additional candidate plants.

Ten plants targeting the *MpTOLa* locus that displayed pronounced phenotypic differences from WT were selected for further molecular characterization.

4.2.2 Molecular screening of the *MpTOLb* locus

A similar molecular screening strategy was applied to the *MpTOLb* locus. The PCR products obtained using Mp5g-PCR-F and Mp5g-PCR-R were analysed by agarose gel electrophoresis and subjected to sequencing using the forward primer. No sequence alterations were detected at the Mp5g1 target site. However, the reverse primer used for the initial amplification was located close to the Mp5g2 target region, limiting the quality and reliability of the sequence obtained around this site. In addition, amplification with the initial primer pair was not consistently successful.

To improve PCR amplification, genomic DNA samples were diluted before PCR to reduce the potential effects of PCR-inhibitory compounds present in the DNA preparations. Several dilution ratios were tested, with 1:5 and 1:6 dilutions generally providing more reliable amplification across samples with initial DNA concentrations ranging from approximately 150 to 500 ng/µL.

A new reverse primer, Mp5g-PCR-R2, was subsequently used in combination with Mp5g-PCR-F to re-amplify the *MpTOLb* locus. However, Mp5g-PCR-R2 was still located relatively close to the Mp5g2 target site and the end of the gene and therefore did not provide a sufficiently extended sequencing region for reliable assessment of mutations at this site. A third reverse primer, Mp5g-PCR-R3, located further downstream of the Mp5g2 target site, was therefore used to extend the

sequencing region and determine whether the identified mutations resulted in a frameshift. A schematic representation of the primers is shown in Figure 13.

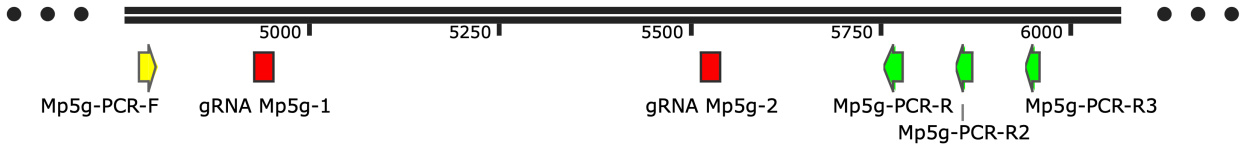


Figure 13: Schematic representation of the primers used for amplification and sequencing of the *MpTOLb* locus. The Mp5g1 and Mp5g2 target sites are indicated in red, the forward primer Mp5g-PCR-F in yellow, and the three reverse primers Mp5g-PCR-R, Mp5g-PCR-R2, and Mp5g-PCR-R3 in green. The reverse primers were progressively positioned further downstream of the Mp5g2 target site to extend the sequencing region and obtain a reliable sequence for the assessment of mutations relative to the WT sequence.

No plants carrying an amplicon substantially shorter than the WT product were identified for the *MpTOLb* locus. Thus, no evidence of the large deletion expected from simultaneous cleavage at the two gRNA target sites was obtained among the screened plants. However, the absence of this deletion did not exclude the presence of smaller insertions or deletions at one or both individual target sites.

The screening strategy was therefore expanded to include a phenotype-guided approach. Plants showing pronounced differences from WT were selected based on overall size, pigmentation, gemma production or absence of gemmae, and thallus morphology, and were subsequently subjected to molecular characterization. Using this phenotype-guided approach, the *MpTOLb* locus was sequenced in 12 plants.

4.3 Characterization of *M. polymorpha MpTOLa* and *MpTOLb* mutant lines

Following the phenotypic screening and molecular analysis described above, only a subset of the selected plants showed sequence alterations at *MpTOLa* or *MpTOLb* consistent with CRISPR/Cas-mediated editing. The identified sequence variants are summarized in Table 11 and Table 12.

Transformant	Plant number	Mutation in position 84 at CDS	Result
Mptola-1	33	1 bp deletion	Frameshift
Mptola-2	53	1 bp deletion	Frameshift

Table 11: Sequence alterations identified in the *MpTOLa locus.*

Transformant	Plant number	Mutation in Mp5g-2 site	Result
Mptolb-1	2	1 bp insertion	Frameshift
Mptolb-2	7	1 bp insertion	Frameshift
Mptolb-3	13	7 bp insertion	Frameshift
Mptolb-4	14	6 bp deletion	No Frameshift
Mptolb-5	15	1 bp deletion	Frameshift
Mptolb-6	27	1 bp deletion	Frameshift
Mptolb-7	68	5 bp deletion	Frameshift
Mptolb-8	73	260 bp deletion	Frameshift
Mptolb-9	86	109 bp insertion, 10 bp deletion	Frameshift

Table 12: Sequence alterations identified in the *MpTOLb* locus.

Among the identified variants, mutant lines carrying deletions and predicted frameshift mutations were selected for further characterization, as these alterations were expected to have a greater potential to disrupt the coding sequence.
Based on these criteria, *Mptola-1* and *Mptola-2* (plants 33 and 53, respectively) and *Mptolb-5*, *Mptolb-6*, and *Mptolb-8* (plants 15, 27, and 73, respectively) were selected for subsequent analyses.

Since *M. polymorpha* is a dioecious species, the sex of the selected plants was determined by PCR using two sex-specific primer pairs: Male-Seq-F/Male-Seq-R and Female_F/Female_R. The PCR products were analysed by agarose gel electrophoresis, and the sex of each plant was assigned based on the presence of the corresponding sex-specific amplicon. The identified sexes are summarized in Table 13.

Transformant	Plant number	Sex
Mptola-1	33	Male
Mptola-2	53	Female
Mptolb-5	15	Female
Mptolb-6	27	Male
Mptolb-8	73	Female

Table 13: Sex of the selected *M. polymorpha* TOL mutant plants.

To determine whether the identified mutations were stably maintained during vegetative propagation, gemmae from the selected plants were propagated to obtain a subsequent generation. Genomic DNA was then extracted from the resulting plants, and the corresponding *MpTOLa* or *MpTOLb* loci were amplified and sequenced. Sequencing confirmed the presence of the mutations previously identified in the parental plants, indicating that the edited sequences were maintained following vegetative propagation.

The identified mutations were further analysed in silico at the protein level to assess their predicted effects on the encoded MpTOLa and MpTOLb proteins. The corresponding WT and mutant protein sequences are shown from Figure 14 to Figure 18. In the sequence alignments, the asterisk indicates a premature stop codon in the translated mutant sequence, while blue highlights the region altered relative to the WT sequence.

MpTOLa WT protein (408 aa)

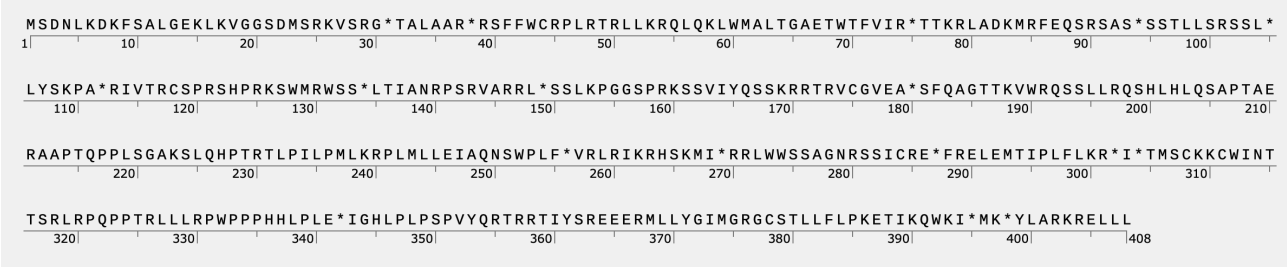


Figure 14: Amino acid sequence of the WT MpTOLa protein. The asterisk indicates a stop codon in the translated mutant sequence.

MpTOLa mutant proteins in *Mptola-1* and *Mptola-2*



Figure 15: Amino acid sequences of the MpTOLa mutant proteins in *Mptola-1* and *Mptola-2*. The asterisk indicates a premature stop codon in the translated mutant sequence. The altered region is highlighted in blue.

The 1-bp deletion identified in *Mptola-1* and *Mptola-2* induces an early frameshift at amino acid position 31 (Figure 14, Figure 15). This results in complete disruption of the protein sequence and

early translation termination. Thus, the mutations identified in *Mptola-1* and *Mptola-2* are predicted to result in loss of protein function. Consequently, essential functional domains, such as the N-terminal VHS domain, which is typically required for ubiquitinated cargo recognition in TOL family proteins, are entirely lost.

MpTOLb WT protein (668 aa)



Figure 16: Amino acid sequence of the WT MpTOLb protein. The asterisk indicates a stop codon in the translated mutant sequence.

MpTOLb mutated proteins in the candidates *Mptolb-5* and *Mptolb-6*:

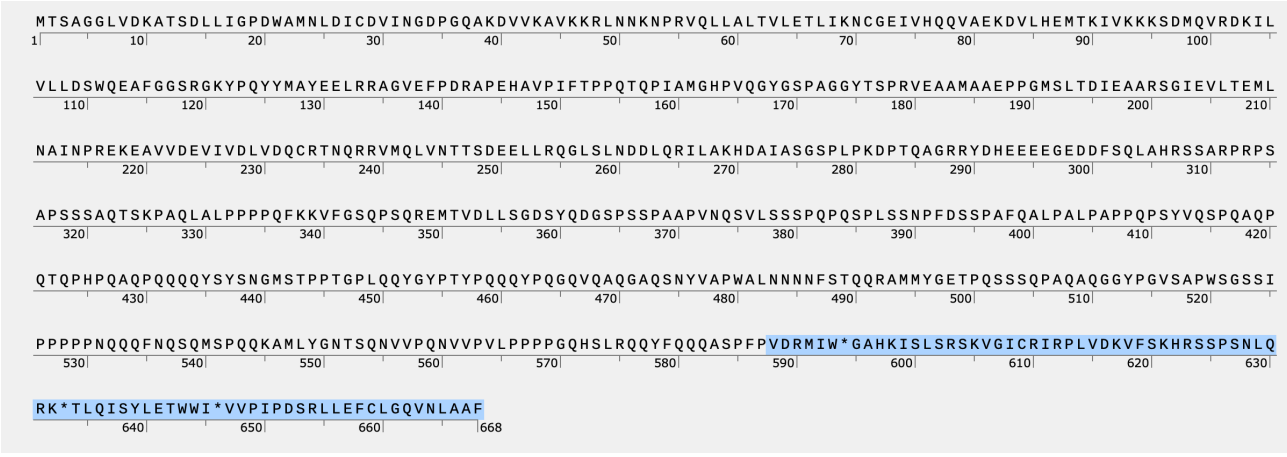


Figure 17: Amino acid sequences of the MpTOLb mutant proteins in *Mptolb-5* and *Mptolb-6*. The asterisk indicates a premature stop codon in the translated mutant sequence. The altered regions are highlighted in blue.

MpTOLb mutated protein in the candidate *Mptolb-8*:

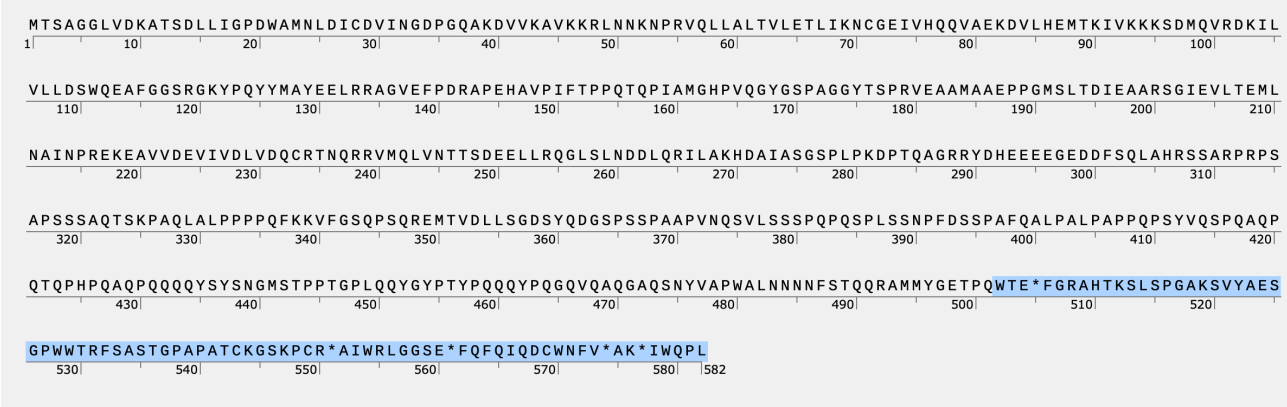


Figure 18: Amino acid sequences of the MpTOLb mutant proteins in *Mptolb-8*. The asterisk indicates a premature stop codon in the translated mutant sequence. The altered regions are highlighted in blue.

The mutations identified in *Mptolb-5*, *Mptolb-6*, and *Mptolb-8* occur in the distal region of the coding sequence, preserving approximately 75% to 89% of the N-terminal sequence (Figure 16, Figure 17, Figure 18). These mutant lines are thus expected to express C-terminally truncated proteins rather than complete nulls.

While the conserved N-terminal region may maintain basal interactions or ubiquitin-binding capacity, the loss of the native C-terminus may impair downstream protein-protein interactions, protein stability, or regulatory phosphorylation sites. Such C-terminal alterations could result in hypomorphic alleles or exert a dominant-negative effect by interfering with the assembly of endogenous ESCRT complexes.

Alternatively, the identified mutations may trigger nonsense-mediated mRNA decay (NMD), leading to degradation of the mutant transcripts and consequently reduced or absent production of the corresponding truncated proteins. This possibility could be tested in the future by quantitative PCR (qPCR) to determine whether transcript levels are reduced in the mutant lines.

Overall, the sequence analysis indicates that the selected *MpTOLa* and *MpTOLb* mutant lines carry mutations predicted to substantially alter the corresponding protein sequences, either through frameshift-induced changes in the downstream amino acid sequence or through loss of the native C-terminal region. However, the actual effects of these mutations on protein stability, localization, and function require experimental validation and cannot be established from sequence analysis alone.

4.4 Phenotypic characterization of *M. polymorpha MpTOLa* and *MpTOLb* mutant lines

Once the stability of the mutations through vegetative propagation had been confirmed, the growth of the selected mutant lines was monitored over time and documented photographically at different developmental stages. The resulting phenotypes were subsequently compared with those of WT plants to identify differences in growth and overall thallus morphology.

Mptola-1 **(Plant 33, Male):**

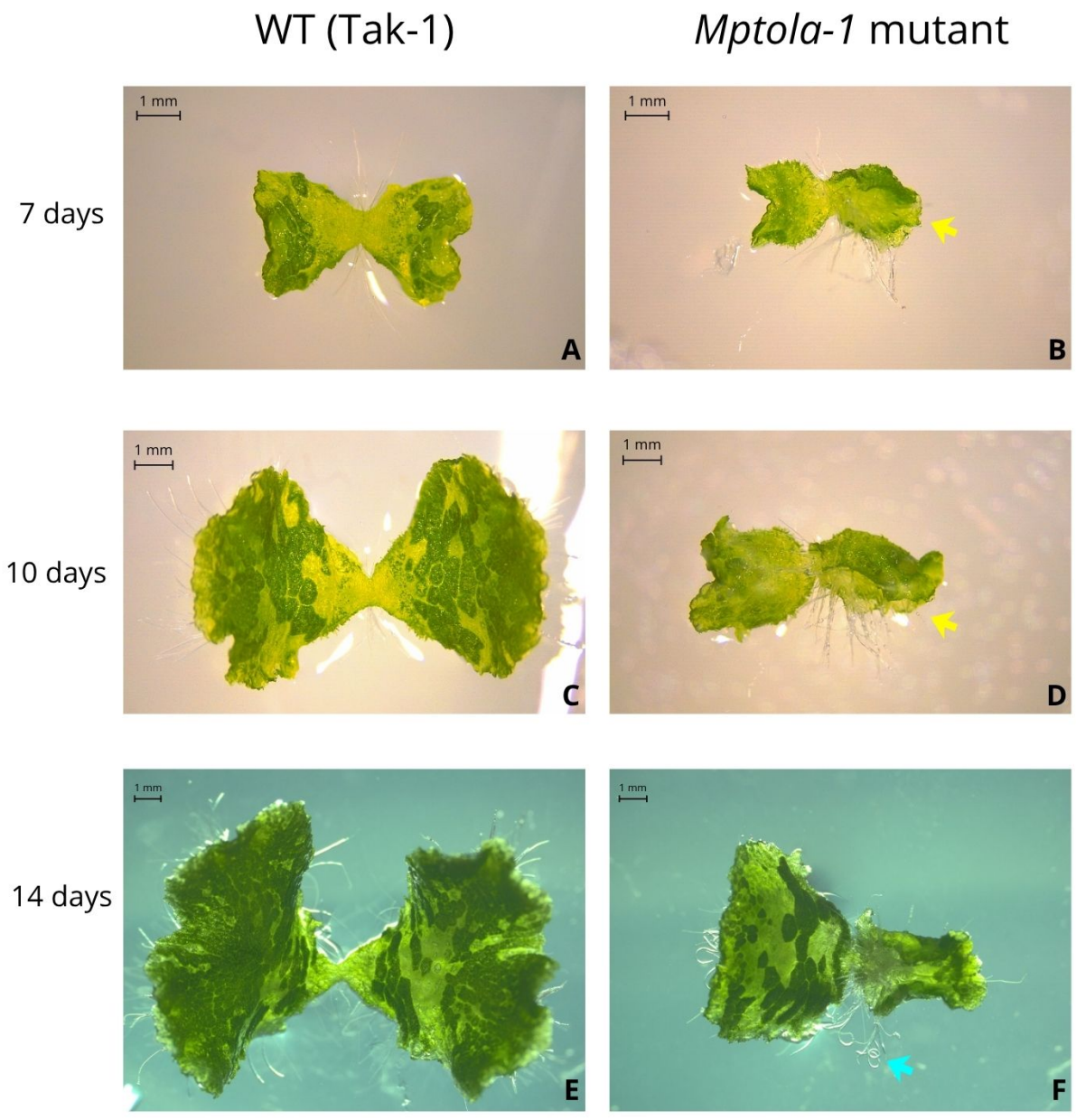


Figure 19: Representative images of a WT and *MpTOLa-1* mutant gemmalings grown for 7, 10, and 14 days. Yellow arrows indicate the 90° rotation of the right thallus lobe; light blue arrows indicate curled rhizoids.

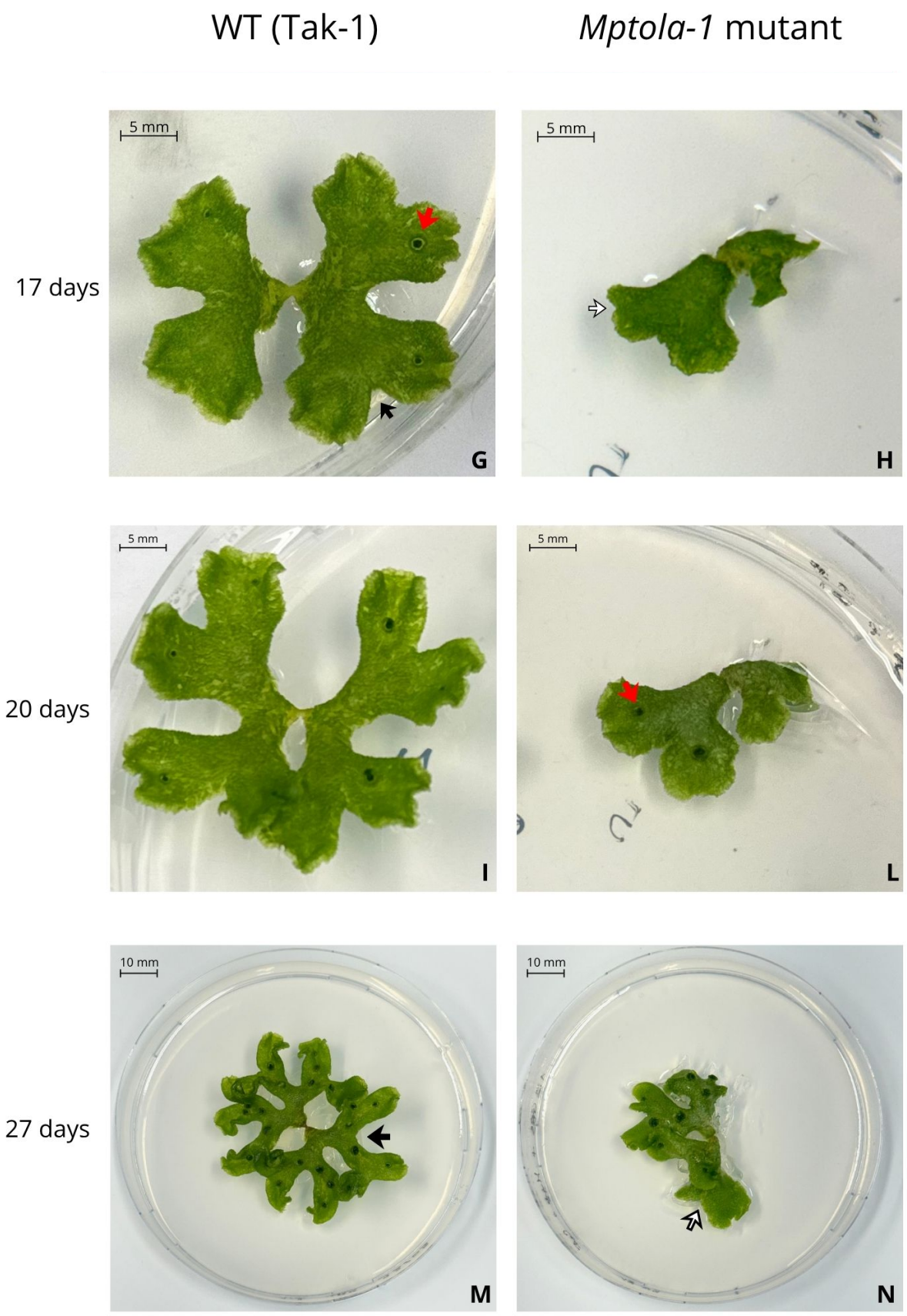


Figure 20: Representative images of a WT and *Mptola-1* mutant gemmaling grown for 17, 20, and 27 days. Red arrows indicate gemma cups; black arrows indicate the WT apical notches; white arrows with black outlines indicate the apical notches in the mutant.

Phenotypic differences between *Mptola-1* and the WT plant were already visible at 7 days after gemma germination (Figure 19A-B). The *Mptola-1* plant was smaller and showed an asymmetric thallus, with a loss of the bilateral symmetry observed in the WT plant (Figure 19B). The right thallus lobe was also rotated by approximately 90° relative to the growth plane (Figure 19B). In addition, the rhizoids showed an agravitropic growth pattern (Figure 19B).

At day 10, the difference in growth between *Mptola-1* and the WT control became more evident, as the mutant plant was smaller and its rhizoids showed a more horizontal growth orientation compared with the WT plant (Figure 19C-D).

At day 14, the rhizoids of *Mptola-1* showed an altered morphology, with curled apical tips (Figure 19F). In contrast, the overall pigmentation of the thallus remained similar to that of the WT plant (Figure 19E-F).

By day 17, the WT plant had developed a mature thallus with distinct apical notches and abundant gemma cups (Figure 20G). At the same time point, the *Mptola-1* plant remained smaller and appeared less developed (Figure 20H). The thallus lobes remained partially fused and lacked the clear apical notch observed in the WT plant, while gemma cups were not yet visible (Figure 20G-H). The thallus also showed a marked curvature (Figure 20H).

Gemma cups became visible in the *Mptola-1* plant around day 20 (Figure 20L).

By day 27, the mutant plant was still considerably smaller than the fully developed Tak-1 control (Figure 20M-N) and showed a curved and hyponastic thallus, together with asymmetric expansion of the two lobes (Figure 20N).

***Mptola-2* (Plant 53, Female):**

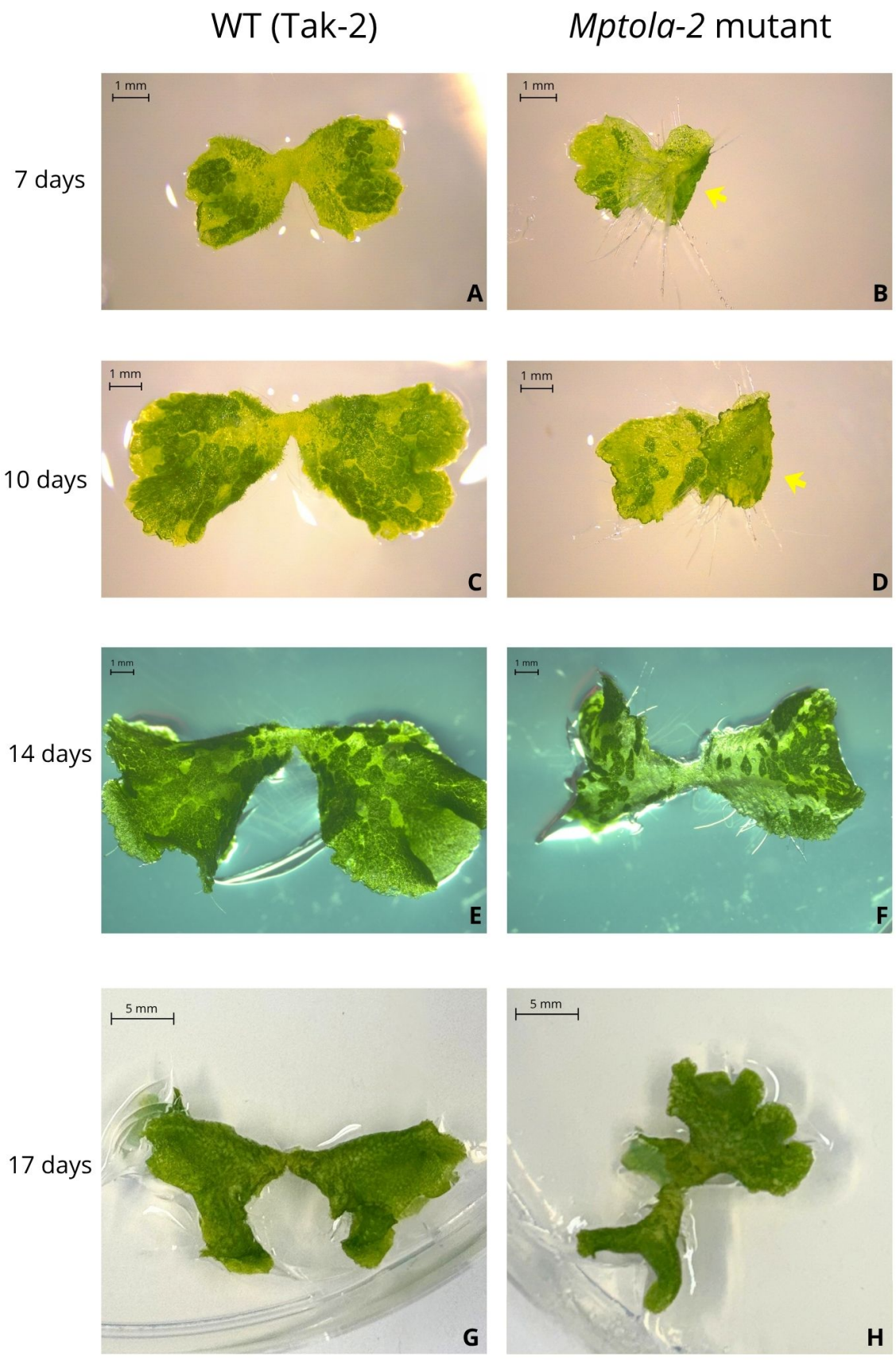


Figure 21: Representative images of a WT and *Mptola-2* mutant gemmalings grown for 7, 10 14 and 17 days. Yellow arrows indicate the 90° rotation of the right thallus lobe.

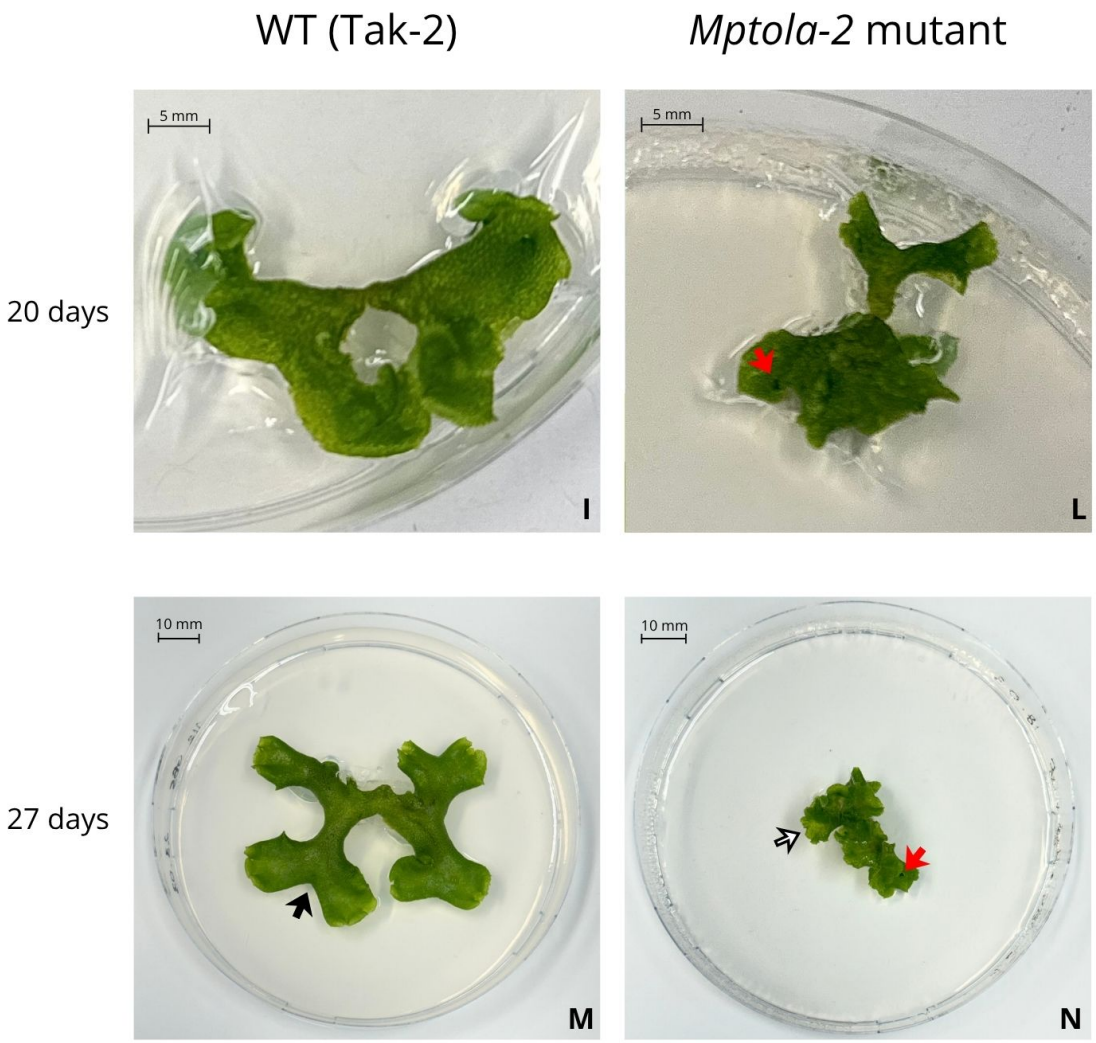


Figure 22: Representative images of a WT and *Mptola-2* mutant gemmalings grown for 20 and 27 days. Red arrows indicate gemma cups; black arrows indicate the WT apical notches; white arrows with black outlines indicate the apical notches in the mutant.

Compared with the Tak-2 female WT control, which naturally showed some growth below the agar surface (Figure 21G, Figure 22I), the *Mptola-2* plant was smaller and showed an approximately 90° rotation of the right thallus lobe from day 7 onwards (Figure 21B, D).

Between days 7 and 14, the thallus of *Mptola-2* also showed lighter green pigmentation than the female WT control (Figure 21A-F).

During the following days, from day 17 (Figure 21) to day 27 (Figure 22), *Mptola-2* showed a different growth pattern compared with the WT plant. Instead of expanding mainly horizontally along the agar surface, the thallus grew more vertically and showed a hyponastic orientation (Figure 22L, N). A difference in developmental timing was also observed. The *Mptola-2* plant started to

form gemma cups around day 20 (Figure 22L), whereas the female WT plant did not develop gemma cups until around day 27 (Figure 22M).

At day 27, the WT plant had developed well-defined apical notches, whereas the *Mptola-2* plant showed a more irregular and undulating apical thallus margin, with less clearly defined notches (Figure 22M-N). Thus, *Mptola-2* showed both altered thallus morphology and an earlier onset of gemma cup formation compared with the female WT control.

***Mptolb-5* (Plant 15, Female):**

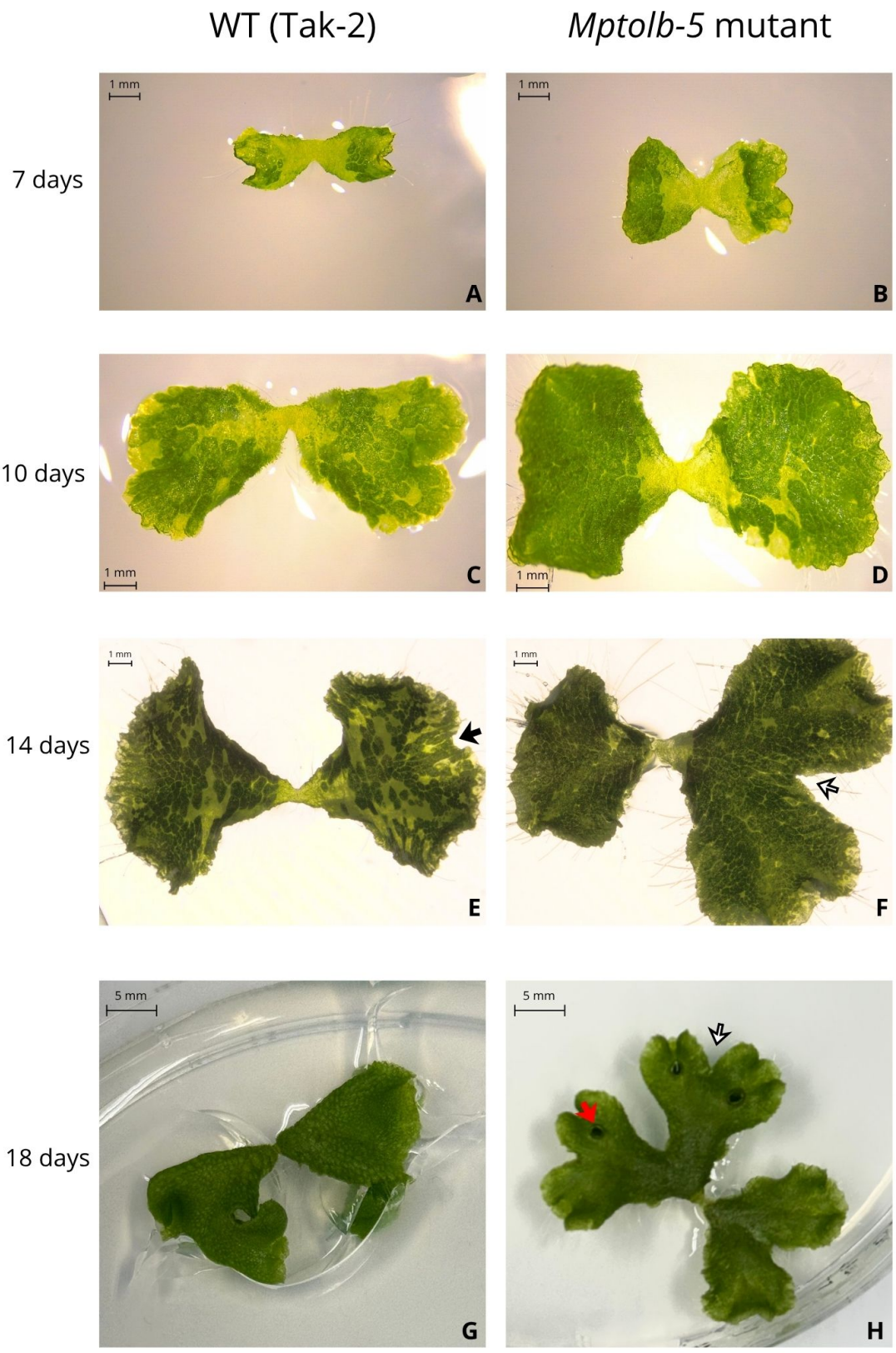


Figure 23: Representative images of a WT and *Mptolb*-5 mutant gemmalings grown for 7, 11, 14 and 18 days. Red arrows indicate gemma cups; black arrows indicate the WT apical notches; white arrows with black outlines indicate the apical notches in the mutant.

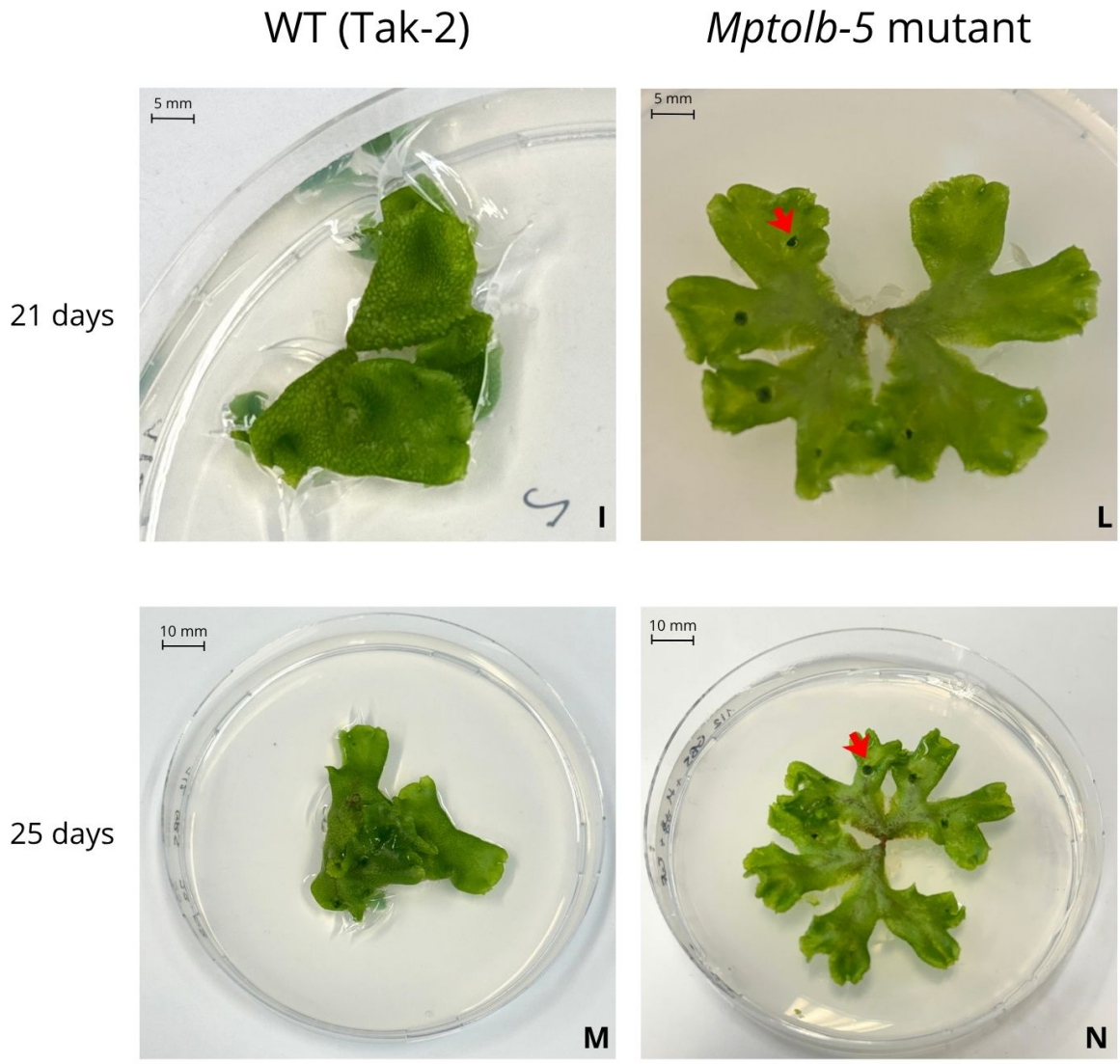


Figure 24: Representative images of a WT and *Mptolb-5* mutant gemmalings grown for 21 and 25 days. Red arrows indicate gemma cups.

From day 7 after gemma germination onwards, the *MpTOLb-5* plant was visibly larger than the Tak-2 female WT control (Figure 23A-H), mainly due to greater width of the thallus lobes rather than increased longitudinal growth. The two lobes of the mutant also showed different rates of development, resulting in an asymmetric thallus (Figure 23F, H).

By day 10, *MpTOLb-5* showed darker pigmentation than the WT plant (Figure 23C-D).

In the WT thallus, the dark green areas corresponding to the photosynthetic air chambers were clearly separated (Figure 23C), whereas in *MpTOLb-5* these areas appeared more closely spaced and less clearly separated, giving the thallus a more uniformly dark appearance (Figure 23D).

By day 14, while the apical notch of the WT plant was still poorly developed (Figure 23E), a clear apical notch had already formed in the more advanced lobe of the mutant plant (Figure 23F).

By day 18, this lobe showed well-defined apical notches and gemma cups (Figure 23H), whereas gemma cups were not yet visible in the Tak-2 control (Figure 23G).

Unlike the *MpTOLb-5* plant, which remained entirely above the agar surface, the female WT plant showed some growth below the agar surface (Figure 23G-H). This growth below the agar surface also made it difficult to clearly assess the development of the WT apical notches (Figure 23G).

By day 25, *MpTOLb-5* still showed a higher number of gemma cups, mainly located on the more developed side of the thallus (Figure 24N). The difference in lobe size became less pronounced as the plant continued to develop (Figure 21B, D, F, H; Figure 24L, N).

In contrast, the WT plant had not yet developed gemma cups at day 25 (Figure 24M).

***Mptolb-6* (Plant 27, Male):**

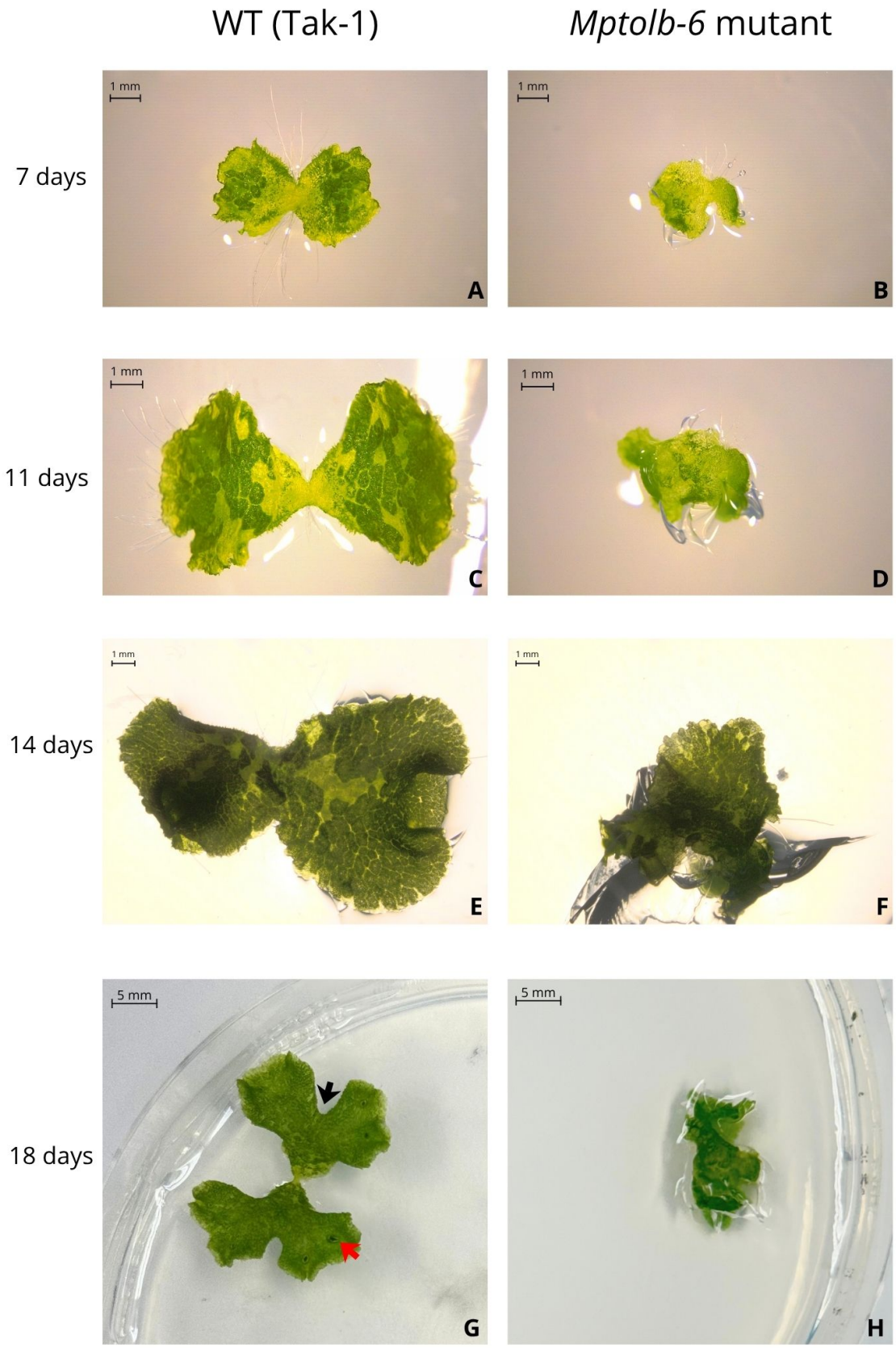


Figure 25: Representative images of a WT and *Mptolb-6* mutant gemmalings grown for 7, 11, 14 and 18 days. Red arrows indicate gemma cups; black arrows indicate the WT apical notches.

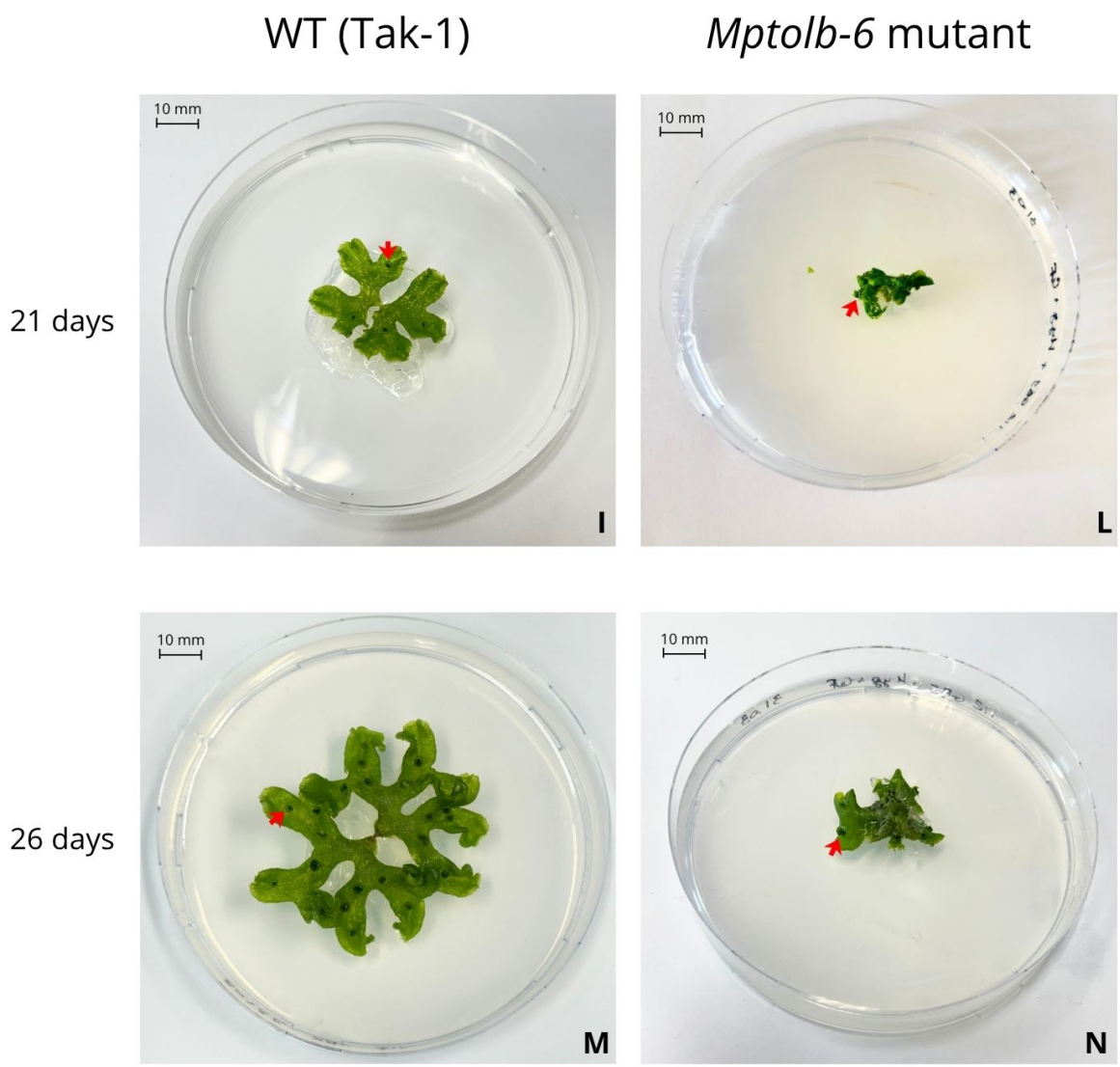


Figure 26: Representative images of a WT and *Mptolb*-6 mutant gemmalings grown for 21 and 26 days. Red arrows indicate gemma cups.

Mptolb-6 showed a strong growth phenotype compared with the WT plant and other *Mptolb* mutants. During the first 11 days, the mutant plant showed reduced growth, lighter green pigmentation, and fewer visible dark green areas associated with the photosynthetic air chambers compared with the WT plant (Figure 25A-D). The thallus of the *Mptolb-6* plant also showed an unusual three-dimensional morphology, with the lobes folded and compacted and growing mainly in a vertical direction rather than remaining flat on the agar surface (Figure 25D).

In contrast to the Tak-1 male WT plant, which generally remained flat on the substrate, the *Mptolb-6* plant also showed partial growth into the agar medium (Figure 25C-F).

By day 18, the WT plant had developed clear and well-defined apical notches, and the first gemma cups had become visible (Figure 26G). In contrast, the apical notches of the *Mptolb-6* plant could not be clearly distinguished due to its compact and folded morphology (Figure 26H).

Mptolb-6 thallus appeared strongly curled and folded onto itself and showed further growth into the agar medium (Figure 26H, L, N). In addition, no gemma cups were visible in the mutant plant at day 18 (Figure 26H).

By day 21, the apical notch was still not clearly developed in the *Mptolb-6* plant (Figure 26L), and the thallus did not show the typical open morphology observed in the WT plant (Figure 26I-L).

However, the mutant plant had developed gemma cups and had started producing gemmae at this time point (Figure 26L).

By day 26, *Mptolb-6* remained considerably smaller than the WT plant and retained a compact and folded morphology (Figure 26M-N).

***Mptolb-8* (Plant 73, Female):**

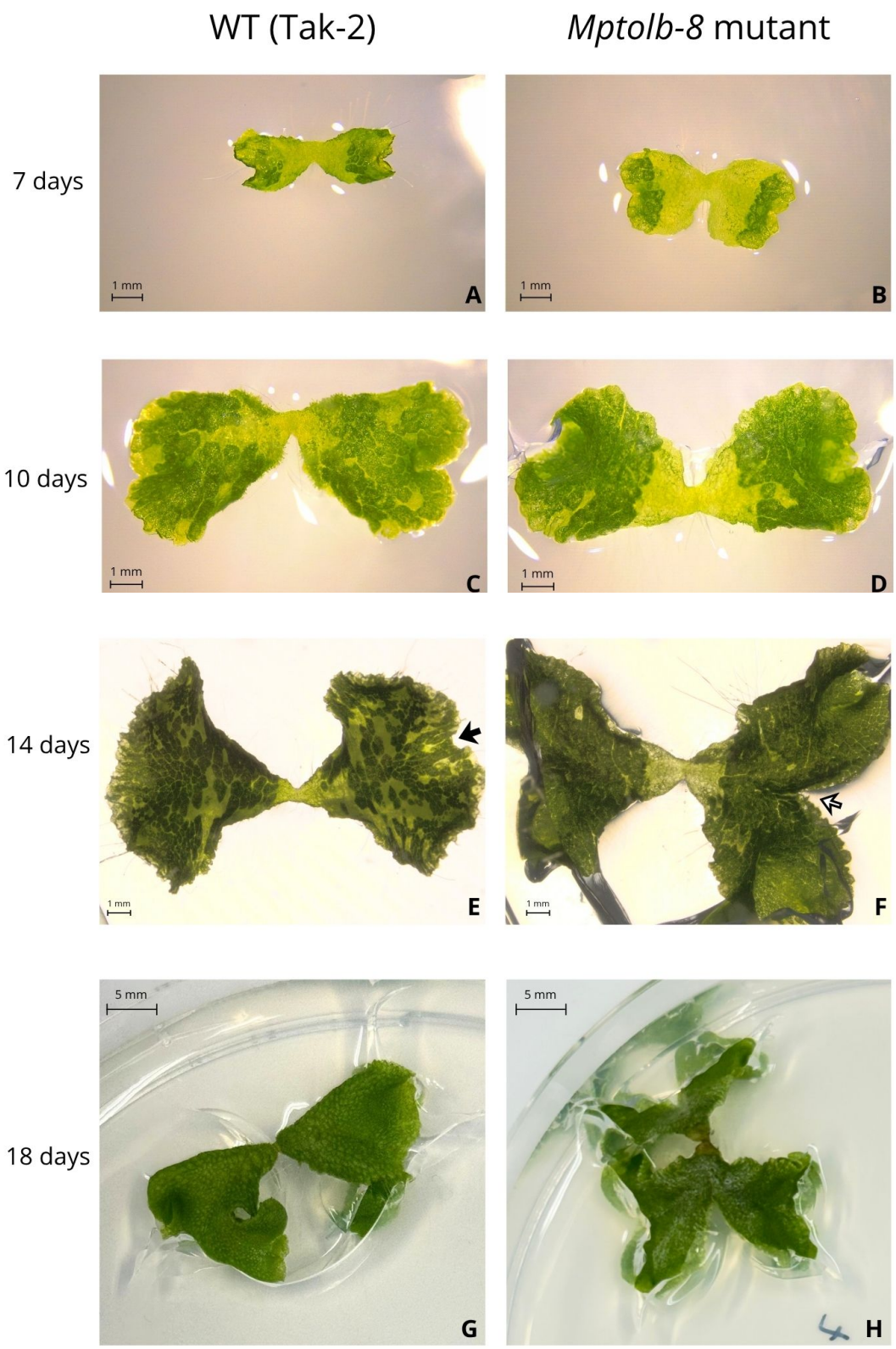


Figure 27: Representative images of a WT and *Mptolb-8* mutant gemmalings grown for 7, 11, 14 and 18 days. Black arrows indicate the WT apical notches; white arrows with black outlines indicate the apical notches in the mutant.

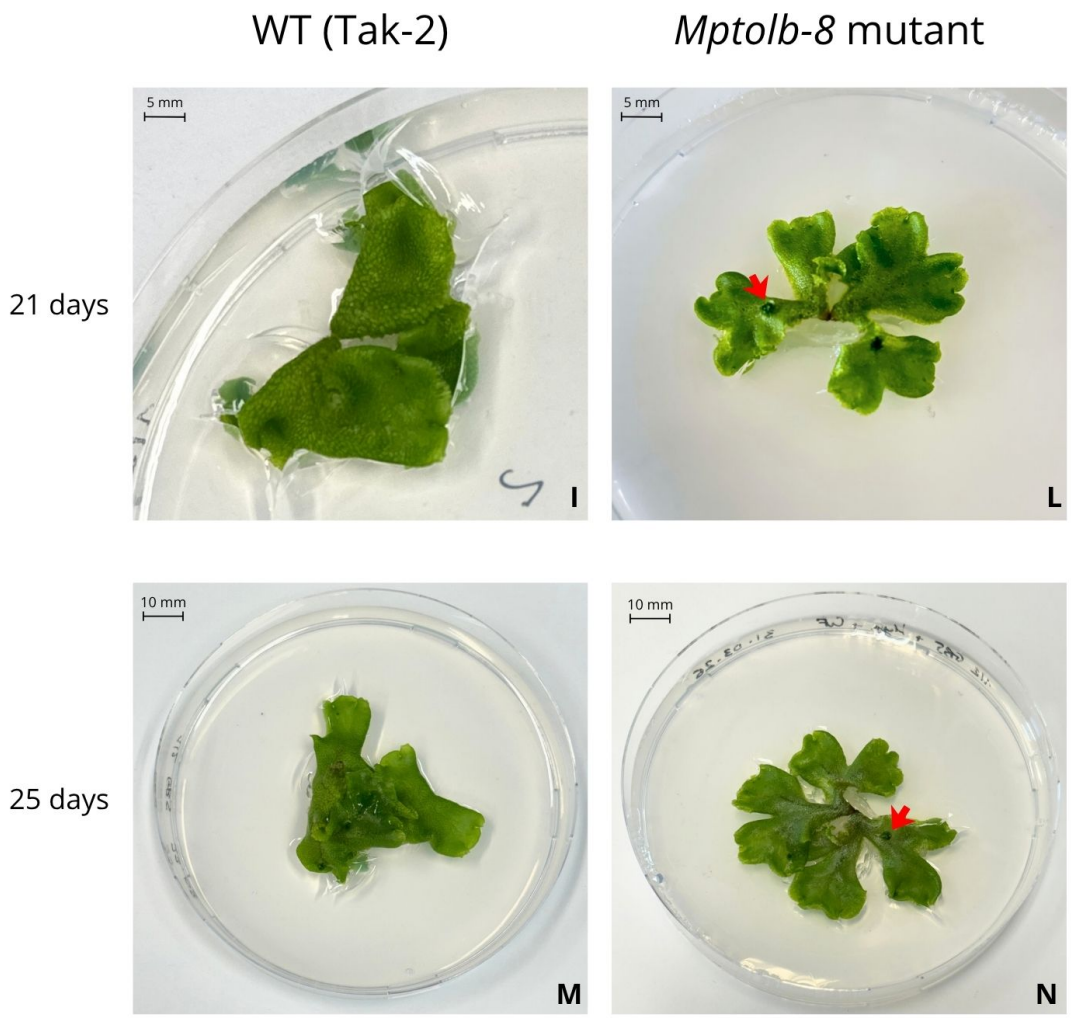


Figure 28: Representative images of a WT and *Mptolb-8* mutant gemmalings grown for 21 and 25 days. Red arrows indicate gemma cups.

During the first 10 days, the overall size of *MpTOLb-8* was comparable to that of the Tak-2 female WT control (Figure 27A-D). However, the distribution of the dark green areas associated with the photosynthetic air chambers appeared different, with these areas being more concentrated towards the distal margins of the thallus rather than being evenly distributed in the mutant plant (Figure 27D).

By day 14, *MpTOLb-8* showed a more pronounced apical notch than the WT plant (Figure 27E-F). By day 18, both the *MpTOLb-8* and WT plants showed some growth into the agar medium (Figure 27G-H). By day 21, *MpTOLb-8* had developed gemma cups and had started producing gemmae (Figure 27L), whereas no gemma cups were visible in the WT plant until day 25 (Figure 28M)

By day 25, the difference in growth morphology between the two plants became more evident. *MpTOLb-8* had expanded across the agar surface, whereas the WT plant remained relatively compact, similarly to the morphology observed in *MpTOLb-5* (Figure 28M).

4.5 Biological Rationale and Putative Molecular Mechanisms

The different phenotypes observed in the *Mptola* and *Mptolb* mutant lines suggest that MpTOL proteins may be involved in several processes that contribute to normal thallus development and growth. In particular, the observed changes in thallus morphology, rhizoid growth, growth direction, and timing of gemma cup formation may be related to alterations in hormone-regulated processes. However, the molecular mechanisms underlying these phenotypes cannot be directly established from the present results and should therefore be considered as possible explanations.

4.5.1 Possible involvement of auxin transport in the growth phenotypes

Several of the observed phenotypes, including loss of thallus symmetry, approximately 90° rotation of one thallus lobe, altered rhizoid growth, and a more vertical or hyponastic growth pattern, could be related to changes in auxin transport. Auxin is involved in the regulation of growth direction and tissue development in *M. Polymorpha,* including rhizoid formation, thallus growth, and dorsiventral development (Flores-Sandoval et al., 2015). The PIN-FORMED protein MpPIN contributes to the establishment of local auxin gradients (Fisher et al., 2023). This is particularly relevant because, in *Arabidopsis thaliana*, TOL proteins have been shown to participate in the sorting of ubiquitinated plasma membrane proteins, including PIN proteins (Korbei et al., 2013).

Mptola-1 and *Mptola-2* showed asymmetric thallus development, including an approximately 90° rotation of one thallus lobe. *Mptola-1* also showed an altered rhizoid morphology, whereas *Mptola-2* and *Mptolb-6* showed a more vertical or hyponastic growth pattern compared with the corresponding WT plants (Flores-Sandoval et al., 2015).

Therefore, mutations in *MpTOLa* or *MpTOLb* could potentially affect the intracellular trafficking of MpPIN and consequently modify its distribution at the plasma membrane. Changes in MpPIN localization could alter local auxin distribution and contribute to the asymmetric growth observed in the *MpTOLa* mutant lines. Similarly, altered auxin distribution could potentially contribute to the differences in growth direction observed in *MpTOLa-2* and *MpTOLb-6*.

4.5.2 Possible role of ABA signalling in developmental timing

The male mutants *Mptola-1* and *Mptolb-6* developed gemma cups later than the corresponding Tak-1 WT controls, whereas the female mutants *Mptola-2*, *Mptolb-5*, and *Mptolb-8* developed gemma cups earlier than the Tak-2 controls.

This difference may be related to a possible link between TOL-dependent trafficking and hormonal signalling. In *Arabidopsis thaliana*, TOL proteins have been implicated in the regulation of ABA signalling through their role in the endosomal trafficking and turnover of components of the ABA signalling pathway (Moulinier-Anzola et al., 2024).

In addition, ABA receptors have been shown to undergo endosomal trafficking and vacuolar degradation through the ESCRT pathway (Belda-Palazón et al., 2016). Therefore, alterations in TOL-dependent trafficking could potentially affect the abundance or localization of ABA-related components and contribute to the differences in developmental timing observed between the mutant and WT plants.

However, the different phenotypes observed in the *MpTOL* mutant lines may also depend on the sex and genetic background of the plants. The female mutant lines *Mptolb-5* and *Mptolb-8*, despite carrying different mutations (1-bp and 260-bp deletions, respectively), showed several similar phenotypic features, particularly in terms of thallus development and earlier gemma cup formation compared with the female Tak-2 WT control.

Plants carrying the same mutation also showed different phenotypes when they belonged to different sexes. This was observed for *Mptolb-5* (female) and *Mptolb-6* (male), as well as for *Mptola-1* (male) and *Mptola-2* (female). In each pair, the plants carried the same 1-bp deletion causing a frameshift, but showed differences in thallus morphology, growth orientation, and developmental timing compared with their respective Tak-1 (male) and Tak-2 (female) WT controls.

Differences in developmental timing were also observed in the laboratory between male and female WT plants. In particular, gemma formation was generally observed earlier in male plants, while it occurred later in female plants. These comparisons should therefore be interpreted together with the molecular characterization of each line, as differences in compensatory mechanisms or physiological responses may also contribute to the observed phenotypes.

4.6 Construction of *MpTOL* Expression Vectors for Cross-Species Functional Analysis

To evaluate cross-species functional complementation and test whether *AtTOLs* can rescue the phenotypes of *Marchantia polymorpha MpTOLa* and *MpTOLb* mutant lines, expression vectors carrying *AtTOL1*, *AtTOL2*, *AtTOL6*, and *AtTOL9* were designed for transformation into *M. polymorpha*.

To promote constitutive expression in *M. polymorpha*, the endogenous *M. polymorpha ELONGATION FACTOR 1α* promoter (*MpEF1ap*) was selected. Therefore, the 35S promoter present in the pH7FWG2 destination vector had to be replaced (Figure 27).

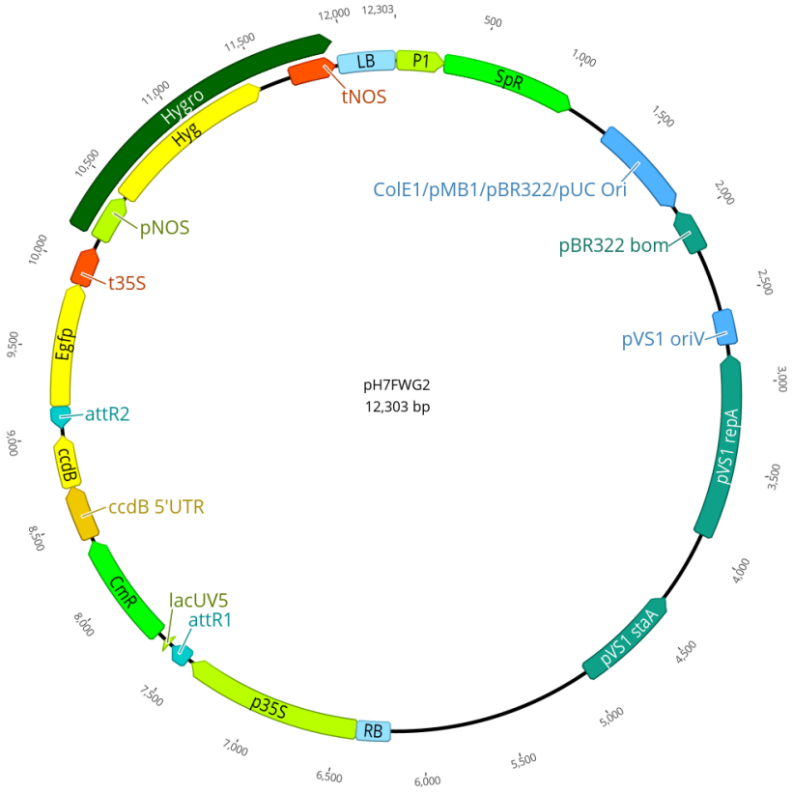


Figure 27: Schematic representation of the pH7FWG2 destination vector. The vector contains the 35S promoter, a Gateway recombination cassette, a GFP coding sequence for C-terminal translational fusion, and a Hyg resistance cassette for plant selection.

The corresponding *MpTOLa* and *MpTOLb* complementation constructs were planned as part of the overall strategy but could not be generated within the experimental period.

4.6.1 Initial Attempts to Replace the 35S Promoter

The initial cloning strategy aimed to replace the 35S promoter in the destination vector pH7FWG2 prior to Gateway LR recombination. The *MpEF1ap* promoter fragment was amplified from pMpGE010 using Q5 High-Fidelity DNA Polymerase with primers MpEF1a_HR_F and MpEF1a_HR_R. These primers introduced flanking *Hind*III and *Spe*I restriction sites at the 5′ and 3′ ends, respectively. Following product purification, the amplicon was doubly digested with *Hind*III-HF and *Spe*I-HF. In parallel, pH7FWG2 was digested with the same enzyme pair and gel-purified to isolate the vector backbone lacking the 35S promoter.
The digested *MpEF1ap* fragment and vector backbone were ligated and transformed into *E. coli* ccdB Survival cells by heat shock.

Although colonies grew on the selective medium, colony PCR screening with MpEF1a_HR_F and MpEF1a_HR_R showed that none of the screened colonies contained the expected *MpEF1ap* insert. Subsequent re-transformation attempts under altered conditions failed to yield verified transformants.

To obtain a sequence-verified source of the *MpEF1ap* fragment, an intermediate TA-cloning strategy was adopted. The *MpEF1ap* promoter was amplified using ALLin™ RPH Polymerase, which adds 3′-A overhangs, and ligated into the pGEM-T vector. The ligation mix was transformed into *E. coli* DH5α cells, and recombinant clones were identified by blue/white selection. Colony PCR screening of 29 white colonies confirmed 26 positive clones. Plasmid DNA from candidate clones was isolated by miniprep and submitted for Sanger sequencing using the M13-21-F and M13-29-R primers. Sequencing confirmed that one clone contained the correct, unmutated *MpEF1ap* sequence.
The *MpEF1ap* promoter was subsequently excised from pGEM-T from the positive clone by *Hind*III/*Spe*I double digestion, gel-purified, and ligated into *Hind*III/*Spe*I-digested pH7FWG2. The ligation was then transformed into both ccdB Survival and DH5α cells. Although primary colonies were recovered on selective medium containing spectinomycin, no clones were verified as positive by colony PCR, and the colonies failed to survive upon subculturing onto fresh selective master plates. Because no stable positive clones were obtained, an alternative cloning strategy was adopted.

4.6.2 Revised Cloning Strategy and Construction of *MpTOL* Expression Vectors

To address vector instability during the initial promoter replacement step, the sequence of the cloning steps was inverted: Gateway LR recombination was performed first to introduce the target coding sequences into the destination vector, followed by promoter replacement.

Gateway LR reactions were set up between entry clones containing *AtTOL1*, *AtTOL2*, *AtTOL6*, and *AtTOL9* and the destination vector pH7FWG2. The LR reaction products were transformed into electrocompetent *E. coli* DH5α cells. Positive transformants were confirmed by colony PCR, isolated by miniprep, and sequenced. Sanger sequencing was performed across each *AtTOL* coding sequence through the downstream GFP region. The sequences confirmed the correct integration of *AtTOL1*, *AtTOL2*, *AtTOL6*, and *AtTOL9*, including their in-frame fusion with GFP and the absence of the native stop codons.

The intermediate constructs (*p35S::AtTOL1-GFP*, *p35S::AtTOL2-GFP*, *p35S::AtTOL6-GFP*, and *p35S::AtTOL9-GFP*) were subsequently subjected to double digestion with *Hind*III and *Spe*I to excise the 35S promoter. Gel electrophoresis revealed an unexpected fragment of approximately 2500 bp instead of the expected 1047 bp. This result suggested a possible structural difference within the 35S promoter region of the vector. Because this fragment represented the excised unwanted region and the flanking *Hind*III and *Spe*I restriction sites remained correct, the backbone fragments could still be gel-purified for downstream use.

In silico restriction analysis revealed internal *Hind*III and *Spe*I recognition sites within the coding sequences of *AtTOL1* and *AtTOL6*, precluding direct promoter replacement using this enzyme pair. Consequently, promoter replacement in the *AtTOL1* and *AtTOL6* constructs was not pursued further. An alternative restriction strategy would be required, for example using an enzyme such as *Sal*I together with primers introducing compatible restriction sites into *MpEF1ap*.

For *AtTOL2* and *AtTOL9*, which lacked internal *Hind*III and *Spe*I sites, the digested backbones were successfully gel-purified and ligated with the *Hind*III/*Spe*I-digested *MpEF1ap* fragment isolated from the positive pGEM-T clone. The ligation products were transformed into *E. coli* DH5α cells by electroporation. Colony PCR screening confirmed the expected construct in all tested *AtTOL2* colonies (16/16) and in 15 of 16 *AtTOL9* colonies.

The final constructs, *MpEF1ap::AtTOL2-GFP* and *MpEF1ap::AtTOL9-GFP*, were recovered from positive colonies and stored as glycerol stocks for subsequent *M. polymorpha* transformation.

5. CONCLUSIONS

This study led to the successful generation, identification, and molecular characterization of stable sequence alterations at both the *MpTOLa* and *MpTOLb* loci in *Marchantia polymorpha* using CRISPR/Cas9 genome editing (Sugano et al., 2014). Among the screened plants, two *Mptola* lines (*Mptola-1* and *Mptola-2*) and three *Mptolb* lines (*Mtolb-5*, *Mptolb-6*, and *Mptolb-8*) were selected for detailed analysis. The mutations were stably inherited following vegetative propagation through gemmae as expected for a dominant haploid gametophyte, in which a mutation is not masked by a second allele (Ishizaki et al., 2016).

Sequence analyses predicted two distinct types of mutations: the *Mptola* lines carried early frameshift mutations predicted to cause loss-of-function, whereas the *Mptolb* lines carried mutations predicted to result in C-terminal truncations, retaining the N-terminal core of the protein. However, their consequences for transcript and protein stability and function remain to be experimentally tested.

The selected mutant lines displayed distinct and severe phenotypic alterations compared with their corresponding WT controls. These included a loss of bilateral symmetry, an approximately 90° axial rotation of thallus lobes, hyponastic vertical growth, and abnormal rhizoid development characterized by horizontal growth and apical curling. Furthermore, differences in developmental timing were observed between sexes. Male mutant lines generally exhibited delayed gemma cup development, whereas female mutant lines showed precocious gemma cup development compared with the corresponding WT controls. Because gemma cup formation is a tightly regulated, hormone-dependent process (Kato et al., 2020), this points to an interaction between TOL function hormonal signaling, which merits separate analysis.

These observations suggest that MpTOLa and MpTOLb may contribute to cell polarity, organogenesis, and developmental timing in *M. polymorpha*. However, the underlying molecular mechanisms underlying these phenotypes remain to be established. In *Arabidopsis thaliana*, TOL proteins act as ubiquitin-receptors at the earliest step of the ESCRT pathway, recognizing ubiquitinated plasma membrane cargo and gating its delivery to the vacuole (Korbei et al., 2013; Moulinier-Anzola et al., 2020). The observed phenotypes may therefore reflect altered endosomal trafficking of plasma membrane proteins.

TOLs have also been shown to influence auxin and ABA signalling in *A. thaliana*. Higher-order tol mutants show defects in auxin-dependent growth, and TOLs mediate the recognition and vacuolar sorting of the auxin efflux carrier PIN2 (Korbei et al., 2013; Moulinier-Anzola et al., 2020). Specific TOLs (TOL2, TOL3, TOL5, and TOL6) additionally attenuate ABA signalling by promoting the degradation of ubiquitinated ABA receptors and transporters (Moulinier-Anzola et al., 2024). In particular, changes in thallus morphology, growth orientation, and rhizoid development are consistent with altered abundance, trafficking or polar localization of the auxin efflux carrier MpPIN1, since auxin transport and signalling control thallus patterning, rhizoid formation, and gemma development in *Marchantia* (Flores-Sandoval et al., 2015; Kato et al., 2015). Similarly, the altered timing of gemma cup formation may be related to changes in auxin and ABA signalling, both of which regulate gemma development and dormancy (Eklund et al., 2015, 2018). If the *Mptol* phenotypes reflect such changes, they would indicate that the coupling of TOL-dependent trafficking to hormone signalling is conserved between bryophytes and angiosperms.

To experimentally validate these hypothetical mechanisms, the generated mutant lines provide a basis for future functional assays. These could include exogenous hormone sensitivity assays and crossing mutant lines with reporter lines to investigate MpPIN localization and auxin responses.
In parallel, this study provided key molecular tools for future functional complementation and cross-species analysis. Expression vectors carrying *AtTOL2* and *AtTOL9* fused to a C-terminal GFP tag under the control of the constitutive promoter *MpEF1ap* (*MpEF1ap::AtTOL2-GFP* and *MpEF1ap::AtTOL9-GFP*) were successfully assembled.
In future studies, these constructs can be used to evaluate whether *Arabidopsis* TOL proteins can complement *M. polymorpha* mutant phenotypes, providing information on the functional conservation of TOL proteins between the two species. Additionally, the GFP tag would allow the subcellular localization of TOL proteins to be investigated in *M. polymorpha* thallus cells.

Completing the remaining constructs *MpEF1ap::AtTOL1-GFP*, *MpEF1ap::AtTOL6-GFP*, *MpEF1ap::MpTOLa-GFP*, and *MpEF1ap::MpTOLb-GFP* would allow a more complete comparison of the different TOL proteins and their ability to complement the *M. polymorpha* mutant phenotypes.
In particular, homologous complementation with the endogenous *MpTOLa* and *MpTOLb* genes could help determine whether the observed phenotypes are directly associated with the CRISPR/ Cas9-induced mutations.

Overall, the mutant lines and molecular tools generated in this study provide a basis for further investigating the roles of MpTOLa and MpTOLb in endosomal trafficking and their possible contribution to plant development in *M. polymorpha* and for evaluating the evolutionary conservation of TOL-mediated sorting in land plants.

6. REFERENCES

- Akutsu, M., Kawasaki, M., Katoh, Y., Shiba, T., Yamaguchi, Y., Kato, R., Kato, K., Nakayama, K., & Wakatsuki, S. (2005). Structural basis for recognition of ubiquitinated cargo by Tom1-GAT domain. *FEBS Letters*, 579(24), 5385–5391. https://doi.org/10.1016/j.febslet.2005.08.076
- Aniento, F., Sánchez de Medina Hernández, V., Dagdas, Y., Rojas-Pierce, M., & Russinova, E. (2022). Molecular mechanisms of endomembrane trafficking in plants. *The Plant Cell*, 34(1), 146–173. https://doi.org/10.1093/plcell/koab235
- Belda-Palazón, B., Rodríguez, L., Fernández, M. A., Castillo, M. C., Anderson, E. M., Gao, C., González-Guzmán, M., Peirats-Llobet, M., Zhao, Q., De Winne, N., Gevaert, K., De Jaeger, G., Jiang, L., León, J., Mullen, R. T., & Rodríguez, P. L. (2016). FYVE1/FREE1 Interacts with the PYL4 ABA Receptor and Mediates Its Delivery to the Vacuolar Degradation Pathway. *The Plant Cell*, 28(9), 2291–2311. https://doi.org/10.1105/tpc.16.00178
- Berger, F., Bowman, J. L., & Kohchi, T. (2016). *Marchantia*. *Current Biology*, 26(5), R186–R187. https://doi.org/10.1016/j.cub.2015.12.013
- Bowman, J. L. (2022). The liverwort *Marchantia polymorpha*, a model for all ages. *Current Topics in Developmental Biology*, 147, 1–32. https://doi.org/10.1016/bs.ctdb.2021.12.009
- Bowman, J. L., Kohchi, T., Yamato, K. T., Jenkins, J., Shu, S., Ishizaki, K., Yamaoka, S., Nishihama, R., Nakamura, Y., Berger, F., Adam, C., Aki, S. S., Althoff, F., Araki, T., Arteaga-Vazquez, M. A., Balasubrmanian, S., Barry, K., Bauer, D., Boehm, C. R., … Schmutz, J. (2017). Insights into Land Plant Evolution Garnered from the *Marchantia polymorpha* Genome. *Cell*, 171(2), 287-304.e15. https://doi.org/10.1016/j.cell.2017.09.030
- Buono, R. A., Leier, A., Paez-Valencia, J., Pennington, J., Goodman, K., Miller, N., Ahlquist, P., Marquez-Lago, T. T., & Otegui, M. S. (2017). ESCRT-mediated vesicle concatenation in plant endosomes. *Journal of Cell Biology*, 216(7), 2167–2177. https://doi.org/10.1083/jcb.201612040
- Clague, M. J., & Urbé, S. (2010). Ubiquitin: Same Molecule, Different Degradation Pathways. *Cell*, 143(5), 682–685. https://doi.org/10.1016/j.cell.2010.11.012
- Dettmer, J., Hong-Hermesdorf, A., Stierhof, Y.-D., & Schumacher, K. (2006). Vacuolar H+-ATPase Activity Is Required for Endocytic and Secretory Trafficking in *Arabidopsis*. *The Plant Cell*, 18(3), 715–730. https://doi.org/10.1105/tpc.105.037978
- Dragwidge, J. M., Wang, Y., Brocard, L., de Meyer, A., Hudeček, R., Eeckhout, D., Grones, P., Buridan, M., Chambaud, C., Pejchar, P., Potocký, M., Winkler, J., Vandorpe, M., Serre, N.,

Fendrych, M., Bernard, A., de Jaeger, G., Pleskot, R., Fang, X., & van Damme, D. (2024). Biomolecular condensation orchestrates clathrin-mediated endocytosis in plants. *Nature Cell Biology,* 26(3), 438–449. https://doi.org/10.1038/s41556-024-01354-6

- Eklund, D. M., Ishizaki, K., Flores-Sandoval, E., Kikuchi, S., Takebayashi, Y., Tsukamoto, S., Hirakawa, Y., Nonomura, M., Kato, H., Kouno, M., Bhalerao, R. P., Lagercrantz, U., Kasahara, H., Kohchi, T., & Bowman, J. L. (2015). Auxin Produced by the Indole-3-Pyruvic Acid Pathway Regulates Development and Gemmae Dormancy in the Liverwort *Marchantia polymorpha*. *The Plant Cell*, 27(6), 1650–1669. https://doi.org/10.1105/tpc.15.00065
- Eklund, D. M., Kanei, M., Flores-Sandoval, E., Ishizaki, K., Nishihama, R., Kohchi, T., Lagercrantz, U., Bhalerao, R. P., Sakata, Y., & Bowman, J. L. (2018). An Evolutionarily Conserved Abscisic Acid Signaling Pathway Regulates Dormancy in the Liverwort *Marchantia polymorpha*. *Current Biology*, 28(22), 3691-3699.e3. https://doi.org/10.1016/j.cub.2018.10.018
- Erpapazoglou, Z., Walker, O., & Haguenauer-Tsapis, R. (2014). Versatile Roles of K63-Linked Ubiquitin Chains in Trafficking. *Cells*, 3(4), 1027–1088. https://doi.org/10.3390/cells3041027
- Fisher, T. J., Flores-Sandoval, E., Alvarez, J. P., & Bowman, J. L. (2023). PIN-FORMED is required for shoot phototropism/gravitropism and facilitates meristem formation in *Marchantia polymorpha. New Phytologist*, 238(4), 1498–1515. https://doi.org/10.1111/nph.18854
- Flores-Sandoval, E., Eklund, D. M., & Bowman, J. L. (2015). A Simple Auxin Transcriptional Response System Regulates Multiple Morphogenetic Processes in the Liverwort *Marchantia polymorpha. PLOS Genetics*, 11(5), e1005207. https://doi.org/10.1371/journal.pgen.1005207
- Frankel, E. B., & Audhya, A. (2018). ESCRT-dependent cargo sorting at multivesicular endosomes. *Seminars in Cell & Developmental Biology*, 74, 4–10. https://doi.org/10.1016/j.semcdb.2017.08.020
- Gao, C., Zhuang, X., Shen, J., & Jiang, L. (2017). Plant ESCRT Complexes: Moving Beyond Endosomal Sorting. *Trends in Plant Science*, 22(11), 986–998. https://doi.org/10.1016/j.tplants.2017.08.003
- Henne, W. M., Buchkovich, N. J., & Emr, S. D. (2011). The ESCRT Pathway. *Developmental Cell*, 21(1), 77–91. https://doi.org/10.1016/j.devcel.2011.05.015
- Herberth, S., Shahriari, M., Bruderek, M., Hessner, F., Müller, B., Hülskamp, M., & Schellmann, S. (2012). Artificial ubiquitylation is sufficient for sorting of a plasma membrane ATPase to the vacuolar lumen of Arabidopsis cells. *Planta*, 236(1), 63–77. https://doi.org/10.1007/s00425-012-1587-0

- Hsiao, A.-S. (2022). Plant Protein Disorder: Spatial Regulation, Broad Specificity, Switch of Signaling and Physiological Status. *Frontiers in Plant Science*, 13. https://doi.org/10.3389/fpls.2022.904446
- Hua, Z., & Vierstra, R. D. (2011). The Cullin-RING Ubiquitin-Protein Ligases. *Annual Review of Plant Biology*, 62(1), 299–334. https://doi.org/10.1146/annurev-arplant-042809-112256
- Hurley, J. H. (2010). The ESCRT complexes. *Critical Reviews in Biochemistry and Molecular Biology*, 45(6), 463–487. https://doi.org/10.3109/10409238.2010.502516
- Husnjak, K., & Dikic, I. (2012). Ubiquitin-Binding Proteins: Decoders of Ubiquitin-Mediated Cellular Functions. *Annual Review of Biochemistry*, 81(1), 291–322. https://doi.org/10.1146/annurev-biochem-051810-094654
- Ishizaki, K., Nishihama, R., Yamato, K. T., & Kohchi, T. (2016). Molecular Genetic Tools and Techniques for *Marchantia polymorpha* Research. *Plant and Cell Physiology*, 57(2), 262–270. https://doi.org/10.1093/pcp/pcv097
- Isono, E., & Kalinowska, K. (2017). ESCRT-dependent degradation of ubiquitylated plasma membrane proteins in plants. *Current Opinion in Plant Biology*, 40, 49–55. https://doi.org/10.1016/j.pbi.2017.07.003
- Kato, H., Ishizaki, K., Kouno, M., Shirakawa, M., Bowman, J. L., Nishihama, R., & Kohchi, T. (2015). Auxin-Mediated Transcriptional System with a Minimal Set of Components Is Critical for Morphogenesis through the Life Cycle in *Marchantia polymorpha*. *PLOS Genetics*, 11(5), e1005084. https://doi.org/10.1371/journal.pgen.1005084
- Kato, H., Yasui, Y., & Ishizaki, K. (2020). Gemma cup and gemma development in *Marchantia polymorpha*. New Phytologist, 228(2), 459–465. https://doi.org/10.1111/nph.16655
- Kohchi, T., Yamato, K. T., Ishizaki, K., Yamaoka, S., & Nishihama, R. (2021). Development and Molecular Genetics of *Marchantia polymorpha*. *Annual Review of Plant Biology*, 72(1), 677–702. https://doi.org/10.1146/annurev-arplant-082520-094256
- Komander, D., & Rape, M. (2012). The Ubiquitin Code. *Annual Review of Biochemistry*, 81(1), 203–229. https://doi.org/10.1146/annurev-biochem-060310-170328
- Korbei, B. (2022). Ubiquitination of the ubiquitin-binding machinery: how early ESCRT components are controlled. *Essays in Biochemistry*, 66(2), 169–177. https://doi.org/10.1042/EBC20210042
- Korbei, B., & Luschnig, C. (2013). Plasma Membrane Protein Ubiquitylation and Degradation as Determinants of Positional Growth in Plants. *Journal of Integrative Plant Biology*, 55(9), 809–823. https://doi.org/10.1111/jipb.12059

- Korbei, B., Moulinier-Anzola, J., De-Araujo, L., Lucyshyn, D., Retzer, K., Khan, M. A., & Luschnig, C. (2013). *Arabidopsis* TOL Proteins Act as Gatekeepers for Vacuolar Sorting of PIN2 Plasma Membrane Protein. *Current Biology*, 23(24), 2500–2505. https://doi.org/10.1016/j.cub.2013.10.036
- Lauwers, E., Jacob, C., & André, B. (2009). K63-linked ubiquitin chains as a specific signal for protein sorting into the multivesicular body pathway. *Journal of Cell Biology*, 185(3), 493–502. https://doi.org/10.1083/jcb.200810114
- Leung, K. F., Dacks, J. B., & Field, M. C. (2008). Evolution of the Multivesicular Body ESCRT Machinery; Retention Across the Eukaryotic Lineage. *Traffic*, 9(10), 1698–1716. https://doi.org/10.1111/j.1600-0854.2008.00797.x
- Liu, H., Shen, C., Hassani, D., Fang, W., Wang, Z., Lu, Y., Zhu, R., & Zhao, Q. (2022). Vacuoles in Bryophytes: Properties, Biogenesis, and Evolution. *Frontiers in Plant Science*, 13. https://doi.org/10.3389/fpls.2022.863389
- Lohi, O., Poussu, A., Mao, Y., Quiocho, F., & Lehto, V.-P. (2002). VHS domain – a longshoreman of vesicle lines. *FEBS Letters*, 513(1), 19–23. https://doi.org/10.1016/S0014-5793(01)03287-2
- Martins, S., Dohmann, E. M. N., Cayrel, A., Johnson, A., Fischer, W., Pojer, F., Satiat-Jeunemaître, B., Jaillais, Y., Chory, J., Geldner, N., & Vert, G. (2015). Internalization and vacuolar targeting of the brassinosteroid hormone receptor BRI1 are regulated by ubiquitination. *Nature Communications*, 6(1), 6151. https://doi.org/10.1038/ncomms7151
- Mattson, T., Bednarek, S., & Johnson, A. (2026). Clathrin-Mediated Endocytosis in Plants: Historical to Modern Advances. *Traffic*, 27(2). https://doi.org/10.1111/tra.70037
- Misra, S., Beach, B. M., & Hurley, J. H. (2000). Structure of the VHS Domain of Human Tom1 (Target of Myb 1): Insights into Interactions with Proteins and Membranes. *Biochemistry*, 39(37), 11282–11290. https://doi.org/10.1021/bi0013546
- Moulinier-Anzola, J., Schwihla, M., De-Araújo, L., Artner, C., Jörg, L., Konstantinova, N., Luschnig, C., & Korbei, B. (2020). TOLs Function as Ubiquitin Receptors in the Early Steps of the ESCRT Pathway in Higher Plants. *Molecular Plant*, 13(5), 717–731. https://doi.org/10.1016/j.molp.2020.02.012
- Moulinier-Anzola, J., Schwihla, M., Lugsteiner, R., Leibrock, N., Feraru, M. I., Tkachenko, I., Luschnig, C., Arcalis, E., Feraru, E., Lozano-Juste, J., & Korbei, B. (2024). Modulation of abscisic acid signaling via endosomal TOL proteins. *New Phytologist*, 243(3), 1065–1081. https://doi.org/10.1111/nph.19904

- Narasimhan, M., Johnson, A., Prizak, R., Kaufmann, W. A., Tan, S., Casillas-Pérez, B., & Friml, J. (2020). Evolutionarily unique mechanistic framework of clathrin-mediated endocytosis in plants. *eLife*, 9. https://doi.org/10.7554/eLife.52067
- Paez Valencia, J., Goodman, K., & Otegui, M. S. (2016). Endocytosis and Endosomal Trafficking in Plants. *Annual Review of Plant Biology*, 67(1), 309–335. https://doi.org/10.1146/annurev-arplant-043015-112242
- Piper, R. C., Dikic, I., & Lukacs, G. L. (2014). Ubiquitin-Dependent Sorting in Endocytosis. *Cold Spring Harbor Perspectives in Biology*, 6(1), a016808–a016808. https://doi.org/10.1101/cshperspect.a016808
- Reynolds, G. D., Wang, C., Pan, J., & Bednarek, S. Y. (2018). Inroads into Internalization: Five Years of Endocytic Exploration. *Plant Physiology*, 176(1), 208–218. https://doi.org/10.1104/pp.17.01117
- Schwihla, M., & Korbei, B. (2020). The Beginning of the End: Initial Steps in the Degradation of Plasma Membrane Proteins. *Frontiers in Plant Science*, 11. https://doi.org/10.3389/fpls.2020.00680
- Shimamura, M. (2016). *Marchantia polymorpha*: Taxonomy, Phylogeny and Morphology of a Model System. *Plant and Cell Physiology*, 57(2), 230–256. https://doi.org/10.1093/pcp/pcv192
- Sugano, S. S., Shirakawa, M., Takagi, J., Matsuda, Y., Shimada, T., Hara-Nishimura, I., & Kohchi, T. (2014). CRISPR/Cas9-Mediated Targeted Mutagenesis in the Liverwort *Marchantia polymorpha* L. *Plant and Cell Physiology*, 55(3), 475–481. https://doi.org/10.1093/pcp/pcu014
- Wang, T., Liu, N. S., Seet, L.-F., & Hong, W. (2010). The Emerging Role of VHS Domain-Containing Tom1, Tom1L1 and Tom1L2 in Membrane Trafficking. *Traffic*, 11(9), 1119–1128. https://doi.org/10.1111/j.1600-0854.2010.01098.x
- Zientara-Rytter, K., & Sirko, A. (2016). To deliver or to degrade – an interplay of the ubiquitin–proteasome system, autophagy and vesicular transport in plants. *The FEBS Journal*, 283(19), 3534–3555. https://doi.org/10.1111/febs.13712